Dynamical Symmetries in Nanophysics

[1]K. Kikoin, [2]M.N. Kiselev and [1,3]Y. Avishai
[1]Department of Physics,
Ben-Gurion University of the Negev,
Beer-Sheva 84105, Israel
[2]Institut für Theoretische Physik,
Universität Würzburg,
D-97074 Würzburg, Germany
[3] Ilse Katz Center for Nano-Technology,
Ben-Gurion University of the Negev,
Beer-Sheva 84105, Israel

Abstract

The main goal of this short review is to demonstrate the relevance of dynamical symmetry and its breaking to one of the most active fields in contemporary condensed matter physics, namely, impurity problems and the Kondo effect. It is intended to expose yet another facet of the existing deep and profound relations between quantum field theory and condensed matter physics. At the same time, the reader should not get the impression that this topics is limited to abstract entities and that it is governed by complicated and sophisticated mathematical structures. On the contrary, it will be shown that many of the concepts introduced below are experimentally relevant. It is one of the rare occasions where the parameters of a dynamical group (e.g the number n of a group $SO(n)$) can be determined experimentally.

We elaborate on the role of dynamical symmetry in a special subdiscipline of condensed matter physics, which enters under the name of correlated impurity problems. It is concerned with the physics which is exposed when the system is composed of strongly correlated localized electrons on the one hand, and itinerant electrons on the other hand. Experimentally, it can be realized in quantum dots and other artificial objects which can be controlled by external parameters such as magnetic fields and gate voltages. Recently, impurity problems have been shown to be realizable also on single molecules. The size of the pertinent impurities then reduces to nanometers and the relevant scientific activity is referred to as nano-science. At low temperatures, the most striking manifestation of impurity problems is the Kondo effect, which is present in bulk systems and, in the last few years, appears to be an indispensable ingredient in nano-science.

The relevant Hamiltonian in impurity problem is a generalized Anderson Hamiltonian which, under certain conditions can be approximated by a generalized spin Hamiltonian encoding the exchange interactions between localized

and itinerant electrons. If the nano-object is, in some sense, simple, (for example, a single localized electron), there is no extra symmetry in the problem. On the other hand, if the quantum dot is complex in some sense, (for example, it contains an even number of electrons or it contains several potential wells) the effective spin Hamiltonian reveals a dynamical symmetry. In particular it includes, beyond the standard spin operators, new sets of vector operators which are the analogues of the Runge-Lenz operator familiar in the physics of the hydrogen atom. These operators induce transitions between different spin multiplets and generate dynamical symmetry groups (usually $SO(n)$) which are not exposed within the bare Anderson Hamiltonian. Like in quantum field theory, the most dramatic aspects of dynamical symmetry in the present context is not its relation with the spectrum but, rather, the manner in which it is broken.

We will review the role of dynamical symmetry and its manifestation in several systems such as planar dots, vertical dots, semiconductor nano-clusters, and complex quantum dots, and show how these dynamical symmetries are broken by exchange interactions with itinerant electrons in the metallic electrodes. We will then develop the concept within numerous physical situations, explaining the concept of dynamical symmetry in Kondo co-tunnelling, including the interesting case of Kondo co-tunnelling in an external magnetic field. As it turns out, the concept of dynamical symmetry is meaningful also in systems out of equilibrium, and the case of dynamical symmetries at finite frequencies will also be addressed.

1 Dynamical and hidden symmetry in quantum mechanics

The concept of symmetry in quantum mechanics has had its golden age in the middle of the last century. In that period the beauty, elegance and efficiency of group theory was used in various branches of physics: classification of hadron multiplets, isospin in nuclear reactions, the orbital symmetry in Rydberg atoms, point-groups in crystallography, translational symmetry in solid state physics, and so on. At the focus of all these studies is the symmetry group of the underlying Hamiltonian. Using the powerful formalism of symmetry operators and their irreducible representations, the energy spectrum of any Hamiltonian with a given symmetry could be found in an elegant and economical way. Exploiting the properties of discrete and infinitesimal rotation and translation operators, general statements about the basic properties of quantum mechanical systems could be formulated in a form of theorems (Bloch theorem, Goldstone theorem, Adler principle, etc). The intimate relation between group theory and quantum mechanics has been exposed in numerous excellent handbooks (see, e.g. [1]).

A somewhat more subtle aspect featuring group theory and quantum mechanics emerged and was formulated later on, that is, the concept of dynamical symmetry. The notion of dynamical symmetry group is distinct from that of the familiar sym-

metry group. To understand this distinction in an heuristic way let us recall that all generators of the symmetry group of the Hamiltonian $\mathcal{H}$ encode certain integrals of the motion, which commute with $\mathcal{H}$. These operators induce all transformations which conserve the symmetry of the Hamiltonian, and may have non-diagonal matrix elements only within a given irreducible representation space of $\mathcal{H}$. On the other hand, dynamical symmetry of $\mathcal{H}$ is realized by transformations implementing transitions between states belonging to *different* irreducible representations of the symmetry group. One may then say that the irreducible representation of the dynamical group of the Hamiltonian requires consideration of the energy spectrum as a whole (see [2] for discussion of various aspects of dynamical symmetries in quantum mechanics).

A special case of dynamical symmetry in quantum mechanics is that of a *hidden* symmetry, where additional degeneracy exists due to an implicit symmetry of the interaction. In particular, such hidden symmetry is a characteristic feature of Coulomb interaction in the hydrogen atom and the isotropic oscillator [3]. This form of hidden symmetry (implemented by the Coulomb interaction) results from an explicit invariance of $1/r$ potentials in a four dimensional energy/momentum space [4], and manifests itself in the degeneracy of states with different orbital angular momentum l.

A mathematically compact and elegant way to describe various kinds of symmetry operations *in many-particle quantum problems* is by means of the so called configuration change operators introduced by J. Hubbard in the context of his seminal work on the "Hubbard model" [5]. These so called Hubbard operators are constructed, in fact, in terms of Dirac's ket/bra operations in the space of eigenvectors $|\Psi\rangle$ of the Hamiltonian $\mathcal{H}$. In other words, let E_Λ be an eigenstate of the Hamiltonian, that is, $(\mathcal{H} - E_\Lambda)|\Lambda\rangle = 0$. Then a configuration changing operator is defined as

$$X^{\Lambda\Lambda'} = |\Lambda\rangle\langle\Lambda'|. \tag{1}$$

Following the accepted terminology, we refer to these operators as *Hubbard operators*. In the original Hubbard model these operators were intended to describe excitations in the narrow electron bands under condition that the on-site Coulomb repulsion exceeds the kinetic energy of electron tunnelling between neighboring sites. Then the Hubbard operators are termed as *Bose-like* if the pairs of states (Λ, Λ') belong to the same charge sector of the Fock space $\{\Lambda\}$ or if the charge of the system N is changed by an even number ΔN as a result of configuration changes $(\Lambda' \to \Lambda)$. In case of an odd ΔN the Hubbard operator is termed as *Fermi-like*. Note that the one-site part $\mathcal{H}_0$ of the Hubbard Hamiltonian and the Dirac's projection operator $\mathcal{P} = |\Psi\rangle\langle\Psi|$ can be rewritten in terms of diagonal Hubbard operators,

$$\mathcal{H}_0 = \sum_\Lambda E_\Lambda |\Lambda\rangle\langle\Lambda| \equiv \sum_\Lambda E_\Lambda X^{\Lambda\Lambda} , \tag{2}$$

$$\mathcal{P} = \sum_\Lambda X^{\Lambda\Lambda}. \tag{3}$$

The algebra of Hubbard operators is determined by the commutation relations

$$[X^{\Lambda_1\Lambda_2}, X^{\Lambda_3\Lambda_4}]_{\mp} = X^{\Lambda_1\Lambda_4}\delta_{\Lambda_2\Lambda_3} \mp X^{\Lambda_3\Lambda_2}\delta_{\Lambda_1\Lambda_4} \tag{4}$$

and the sum rule

$$\sum_{\Lambda} X^{\Lambda\Lambda} = 1. \tag{5}$$

Here the sign $-$ or $+$ is chosen for "Bose-like" and "Fermi-like" operators respectively. If at least one operator in the brackets is Bose-like, the minus sign prevails. Spin flips and electron-hole excitations are examples of Bose-like configuration changes, and addition or removal of electron to the system implies a Fermi-like configuration change. The algebra of Hubbard operators is predetermined by the right-hand side of Eq. (4). If the commutation relations form a closed set of equations, one may speak of an algebra, which reflects the dynamical symmetry of the manifold $\{\Lambda\}$.

To characterize the dynamical symmetry of a quantum mechanical object in terms of Hubbard operators, we consider a system described by a Hamiltonian $\mathcal{H}_0$ whose eigenstates $|\Lambda\rangle = |M\mu\rangle$ form a basis for an irreducible representation of some Lie group $\mathsf{G_0}$. It should be emphasized that the interaction is included in $\mathcal{H}_0$. Using the commutation rules (4), one easily finds that

$$[X^{\Lambda\Lambda'}, \mathcal{H}_0] = -(E_M - E_{M'})X^{\Lambda\Lambda'}. \tag{6}$$

for the Hamiltonian (2). The Hubbard operators $X^{\Lambda\Lambda'}$, which describe transitions between states belonging to the same irreducible representation with $E_M = E_{M'}$, commute with the Hamiltonian and, according to the general theory of quantum mechanical symmetries, they form generators of the symmetry group of the Hamiltonian $\mathcal{H}_0$. If the states Λ and Λ' belong to different irreducible representations of the group $\mathsf{G_0}$, the corresponding operators $\widetilde{X}^{\Lambda\Lambda'}$ do not commute with $\mathcal{H}_0$. The whole set of operators $X^{\Lambda\Lambda'}$ and $\widetilde{X}^{\Lambda\Lambda'}$ form a closed algebra, provided the Hamiltonian $\mathcal{H}_0$ possesses the definite dynamical symmetry group $\mathsf{D_0}$. An interesting case (hidden symmetry) emerges if the interaction part of $\mathcal{H}_0$ results an additional degeneracy of states belonging to different irreducible representations M and M': Certain linear combinations of Hubbard operators, which describe the corresponding transitions form a set of vector operators characterizing the hidden symmetry of the system. This scenario of emergence of new operators due to the special form of the interaction is analogous to the appearance of the Runge-Lenz vector operator, which describes the hidden $SO(4)$ symmetry of the manifold of bound states (closed orbits) in an attractive Coulomb potential. These operators do not appear explicitly in the Hamiltonian $\mathcal{H}_0$, but rather, enter the Casimir relation, which describe the symmetry invariants. Another manifestation of dynamical symmetry arises when an accidental degeneracy of eigenstates occurs, which does not reflect the symmetry of the Hamiltonian.

Leaving more detailed discussion of the origin of hidden and dynamical symmetries for the last chapter containing the mathematical Addendum, we briefly describe here several examples of Hamiltonians which exhibit definite dynamical symmetry. A simple nontrivial Hamiltonian whose associated dynamical symmetry is characterized by a non-Abelian Lie group is that governing the physics of a pair of electron spins coupled by an exchange interaction. This Hamiltonian describes, for example the spin spectrum of hydrogen molecule, as well as spin dimers which are constituents of various complex molecules, spin ladders, etc. The pertinent spectrum of spin excitations consists of a singlet E_S and a triplet E_T. The energy gap between these states is due to exchange interaction $J = \Delta E_{TS} = E_T - E_S$, which can either be positive (antiferromagnetic coupling) or negative (ferromagnetic coupling). The dynamical symmetry of the $\{S, T\}$ manifold is that of the $SO(4)$ group. Two vectors generating this group are constructed by means of Hubbard operators (6) in the following way:

$$\begin{aligned} S^+ &= \sqrt{2}\left(X^{10} + X^{0-1}\right),\ S^z = X^{11} - X^{-1-1}. \\ R^+ &= \sqrt{2}\left(X^{1S} - X^{S-1}\right),\ R^z = -\left(X^{0S} + X^{S0}\right). \end{aligned} \tag{7}$$

Here $\mathbf{S}$ is the spin 1 operator, while the second vector $\mathbf{R}$ describes S/T transitions. Its appearance is due to dynamical symmetry of a *spin rotator*. Below we call operators of this type R-operators The corresponding Lie algebra o_4 is exhausted by the commutation relations

$$[S_\alpha, S_\beta] = ie_{\alpha\beta\gamma}S_\gamma,\ [R_\alpha, R_\beta] = ie_{\alpha\beta\gamma}S_\gamma,\ [R_\alpha, S_\beta] = ie_{\alpha\beta\gamma}R_\gamma. \tag{8}$$

Here (α, β, γ are Cartesian coordinate indices, and $e_{\alpha\beta\gamma}$ is the anti-symmetric Levi-Civita tensor). These two vector operators are orthogonal, $\mathbf{S} \cdot \mathbf{R} = 0$, and the representation is fixed by the Casimir operator is $\mathbf{S}^2 + \mathbf{R}^2 = 3$. In terms of these operators the Hamiltonian $\mathcal{H}_0$ (2) with $\Lambda = S, T\mu$, and $\mu = 0, \pm 1$ acquires the form

$$\mathcal{H}_0 = \frac{1}{2}\left(E_T\mathbf{S}^2 + E_S\mathbf{R}^2\right) + Const. \tag{9}$$

In this simple Hamiltonian all states belong to the same spin sector of the Fock space, $N = 1, \Delta N = 0$.

The second example is again concerned with an elementary object, the Wannier-Mott exciton. It is also characterized by transitions with $\Delta N = 0$. Here the manifold $\{\Lambda\}$ consists of the ground state (completely occupied valence band and no excitations, $\Lambda = G$ with $N = 0$) and two excitonic states (bound electron-hole pair in singlet and triplet states, $\Lambda = S, T\mu$). The system of Hubbard operators describing two singlets, one triplet and all allowed transitions between these states generate (via linear combinations) the group $SO(5)$. Here, beside the vector $\mathbf{S}$ describing the triplet exciton, there are two R-vectors $\mathbf{R_1}, \mathbf{R_2}$ and a scalar operator A describing G/T, S/T and G/S transitions. Altogether, there are ten operators

whose linear combinations generate the group $SO(5)$. Explicitly, these generators are expressed in terms of Hubbard operators as follows:

$$\begin{aligned} R_1^+ &= \sqrt{2}\left(X^{1G} - X^{G1}\right), \quad R_{1z} = -\left(X^{0G} + X^{G0}\right), \\ R_2^+ &= \sqrt{2}\left(X^{1S} - X^{S1}\right), \quad R_{2z} = -\left(X^{0S} + X^{S0}\right), \\ A &= i(X^{GS} - X^{SG}). \end{aligned} \tag{10}$$

To close the algebra the commutation relations (8) which are valid for $R_{l\alpha}$ $(l = 1, 2)$ should be completed by

$$\begin{aligned} &[R_{l\alpha}, R_{1\beta}] = i\delta_{\alpha\beta}A, \\ &[A, R_{l\alpha}] = iR_{1\alpha}, \quad [A, S_{l\alpha}] = 0. \end{aligned} \tag{11}$$

The system of commutation relations (8), (11) is that of the o_5 algebra, and the manifold $\{G, S, T\}$ obeys an $SO(5)$ dynamical symmetry. The Casimir operator determining the pertinent representation of the $SO(5)$ group in this case is $\mathbf{S}^2 + \mathbf{R}^2 + \mathbf{R_1}^2 + A^2 = 4$. In terms of these operators the exciton Hamiltonian $\mathcal{H}_0$ acquires the form

$$\mathcal{H}_0 = \frac{1}{2}\left(E_G\mathbf{R}_1^2 + E_T\mathbf{S}^2 + E_S\mathbf{R}^2\right) + Const. \tag{12}$$

Our last example of a relatively simple Hamiltonian possessing dynamical symmetry is the s-shell of a hydrogen atom (or hydrogen-like impurity in semiconductor), with a neutral state H^0 and ionized states $H^{\pm}$ included in the manifold of eigenstates. Now the index Λ acquires four values, $\Lambda = 0, \sigma, 2$. Here $\Lambda = 0$ stands for an empty s-shell (positive ion H^+), $\Lambda = \sigma = \uparrow, \downarrow$ corresponds to the neutral state H^0 occupied by an electron with spin σ, and $\Lambda = 2$ means double electron occupation (negative ion H^+). In this system sixteen operators inducing transitions within a given charge sector (that is, $X^{\sigma\sigma'}, X^{00}, X^{22}$) as well as those with $\Delta N = \pm 1$ (namely, $X^{\sigma 0}, X^{\sigma 2}, X^{0\sigma}, X^{2\sigma}$) and $\Delta N = \pm 2$ (explicitly X^{20}, X^{02}) are involved in the set of generators of the dynamical group $SU(4)$. This generic model is interesting *per se*, but it also plays an important role in the physics of strongly correlated electron systems. Indeed, the Hamiltonian $\mathcal{H}_0$ (2) with $\Lambda = 0, \sigma, 2$ describes the "elementary cell" of the famous Hubbard Hamiltonian [5], and its symmetry properties are the key ingredient for studying the structure of its excitation spectrum.

In many generic situations, the state $\Lambda = 2$ is quenched by strong Coulomb repulsion between two electrons occupying the elementary shell. The dynamical group of this reduced Hamiltonian is the group $SU(3)$ with eight generators (two vectors, $\mathbf{R}_1$, and $\mathbf{R}_2$ and two scalars A^+ and A^-):

$$\begin{aligned} R_1^z &= \frac{1}{2}\left(X^{00} - X^{\uparrow\uparrow}\right), \quad R_1^+ = X^{0\uparrow}, \\ R_2^z &= \frac{1}{2}\left(X^{00} - X^{\downarrow\downarrow}\right), \quad R_2^+ = X^{0\downarrow} \\ A^+ &= \frac{\sqrt{3}}{2}X^{\uparrow\downarrow}, \quad A^- = \frac{\sqrt{3}}{2}X^{\downarrow\uparrow}, \end{aligned} \tag{13}$$

The closed u_3 algebra is given by the following commutation relations:

$$
\begin{aligned}
&[R_i^z, R_i^\pm] = \pm R_i^\pm, \quad [R_i^+, R_i^-] = 2R_i^z, \quad i = 1, 2 \\
&[R_1^z, A^\pm] = \mp\frac{1}{2}A^\pm, \quad [R_2^z, A^\pm] = \pm\frac{1}{2}A^\pm \\
&[R_1^+, A^+] = \frac{\sqrt{3}}{2}R_2^+, \quad [R_1^-, A^-] = -\frac{\sqrt{3}}{2}R_2^-, \\
&[R_2^+, A^-] = \frac{\sqrt{3}}{2}R_1^+, \quad [R_2^-, A^+] = -\frac{\sqrt{3}}{2}R_1^-, \\
&[R_1^-, A^+] = [R_1^+, A^-] = [R_2^-, A^-] = [R_2^+, A^+] = 0, \\
&[A^+, A^-] = \frac{3}{2}(R_2^z - R_1^z).
\end{aligned} \tag{14}
$$

The Casimir operator is determined as $\mathbf{R}_1^2 + \mathbf{R}_2^2 + A^+A^- + A^-A^+ = 3/2$. In terms of the above operators the Hamiltonian (2) with $\Lambda = 0, \uparrow, \downarrow$, acquires the following form:

$$
\mathcal{H}_0 = \frac{4}{3}E_0(\mathbf{R}_1^2 + \mathbf{R}_2^2) + \frac{4}{3}E_1(A^+A^- + A^-A^+) + Const. \tag{15}
$$

Here $E_1 = E_\uparrow = E_\downarrow$ (in the absence of an external magnetic field). A similar u_3 algebra can be constructed for the case where the states $\Lambda = 2, \uparrow, \downarrow$ are included in the reduced manifold. If all four states are included in the manifold, the dynamical group is $SU(4)$.

In the above examples we formally analyzed the dynamical symmetry of several simple Hamiltonians without discussing concrete physical situations where this symmetry may be revealed. One may find other model systems possessing $SO(n)$ and $SU(n)$ symmetries (see, e.g., [6]), but the above examples illustrate clearly the general principles of the theory. It is obvious that transitions described by Hubbard operators X may be activated only due to the presence of an external perturbation, which breaks the symmetry of the Hamiltonian $\mathcal{H}_0$. Such perturbation may affect the low-energy part of the spectrum. Possible physical mechanisms involve, for example, an interaction with external reservoirs (roughly speaking, a reservoir is a thermal bath with continuous spectrum).

Another example of a symmetry breaking perturbation which activates a dynamical symmetry is the inclusion of an elementary cell described by the Hamiltonian $\mathcal{H}_0$ into a ladder or a lattice. In both cases the symmetry violation is characterized by a definite energy scale $\delta\varepsilon$, and only states separated by an energy gaps $\Delta \leq \delta\varepsilon$ from the ground state are involved in the dynamical processes. External magnetic field may influence the dynamics of the system by introducing an accidental symmetry in the spectrum of $\mathcal{H}_0$. The high-energy part of the spectrum may be activated by a time-dependent external field, both electric and magnetic. If this field is characterized by a frequency Ω, then those states with $\Delta \sim \hbar\Omega$ are involved.

It is important to emphasize that a quantum mechanical object with rich enough energy spectrum manifests different types of dynamical symmetry in different experiments. For example, transitions between neighboring charge sectors may be

involved in spin-related phenomena only as virtual processes. Electron hopping from site to site in a ladder or a lattice involves transitions with $\Delta N = 1$ and, maybe spin reversals. Resonance excitation excites only inter-level transitions with definite energy difference, etc. From the group-theoretical point of view, this "dynamical ambivalence" follows from the fact that the dynamical groups $SO(n)$ and $SU(n)$ with $n > 2$ may be presented as a product of several simple groups, and the corresponding algebras may be presented as direct sums of several subalgebras. This representation is not unique, and the choice of factorization procedure depends on the type of interaction breaking the symmetry of the Hamiltonian $\mathcal{H}_0$. Several examples of such reduction will be demonstrated below.

Physical systems of nanometer size appear to be excellent candidates for investigating dynamical symmetry effects. First, one may select a few-particle nano-object with definite quantum-mechanical symmetry and an easily calculable energy spectrum and describe it by the Hamiltonian $\mathcal{H}_0$. Second, the interaction of this object with environment may be changed and controlled by means of various external fields. Third, one may fabricate artificial nano-objects with non-trivial symmetry properties and thus, model numerous structures which cannot be found in natural atoms, molecules or crystals.

The aim of this short review is to analyze the symmetry properties of *quantum dots* with due emphasis on the concept of dynamical symmetry. Quantum dots are nanometer size objects confining a few number of electrons, which are fabricated by means of advanced technologies from semiconductor materials. Both shape and size of quantum dot can be controlled and varied. The quantum dot is usually integrated within an electrical circuit, and the leads or wires connecting the quantum dot with a voltage source partially play the role of electron reservoirs or thermal baths. The number of electrons in a quantum dot may be easily tuned by a gate voltage, and there is no principal difficulty in applying an external magnetic field in any desired direction. Besides, one may fabricate complex quantum dots . A complex quantum dot consists of several (simple or elementary) dots with possible electron tunnelling and/or electrostatic interaction between them. A special example (which we discuss in the next section)is a periodic array of self-assembled quantum dots.

2 Nanostructures as artificial atoms and molecules

Nanosize quantum dots with controllable occupation and variable configurations are ideal objects for studying numerous physical manifestations of dynamical symmetry. Recall that a quantum dot is an artificial structure, which consists of finite number of electrons confined within a tiny region of space. If the electron de Broglie wavelength (~ 13 nm) exceeds the confinement radius, the energy spectrum of electrons in the dot is discrete. As a result, the dot can be treated as a "zero-dimensional artificial atom".

These nano-objects may be fabricated in numerous ways. Nanosize silicon micro-

crystallites embedded in a matrix of amorphous SiO_2 [7] are examples of quantum dots obtained by means of three-dimensional quantum confinement. Nanocrystallites preserving the structure of bulk elemental, III-V and II-VI semiconductors were synthesized by the methods of colloidal chemistry [8]. Defect-free quantum dots of various shapes can be grown as islands built in highly strained host semiconductors [9]. In the latter case, quantum dots may form self-assembled periodic or nearly periodic two-dimensional structures. Quantum dots may be fabricated also by imposing confining electrodes on two-dimensional electron gas formed near the interface of heterostructures [11]. Such structures are widely used in the experimental studies of single electron tunnelling and related many-body effects. Quantum dot devices may be prepared in a form of disks or pillars (vertical quantum dots) [10]. In this case they preserve the cylindrical symmetry, and the electron energy spectrum acquires the two-dimensional shell structure analogous to the three-dimensional shell structure of "natural" atoms. Another example of artificial quantum object is a nanoscale ring [12].

Further technological advance enabled fabrication of more sophisticated nano-objects such as (for example) double quantum dots [13]. By this we mean a quantum dot consisting of two wells coupled by electrostatic and/or tunnelling interaction. In the same manner that a simple quantum dot is considered as an artificial atom, a complex structure such as double quantum dot can be looked upon as an artificial molecule. The closest natural analog is the hydrogen molecule H_2 or the corresponding molecular ions $H_2^{\pm}$. As far as further complexity is concerned, there is no principal obstacles against fabrication of composite quantum dots consisting of more than two wells. They are the artificial analogs of complex natural molecules.

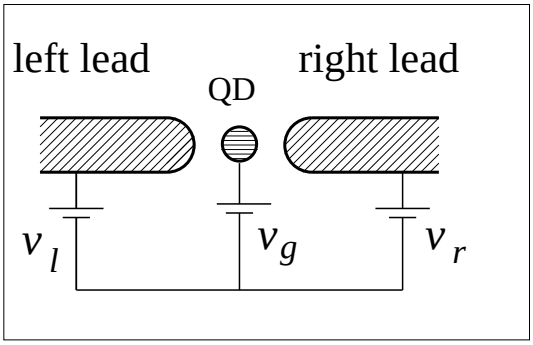

Figure 1: Equivalent circuit for a QD connected to two metallic leads (left and right). Bias voltage is $v_b = v_l - v_r$, gate voltage v_g regulates the number of electrons in the QD.

The main experimental tool used for studying of electronic properties of QD is tunnelling current measurements where the nano-object is incorporated in an electric circuit (Fig. 1). From the quantum statistical point of view such a setup can be

treated as an artificial atom or molecule in a tunnel contact with electron reservoirs (metallic leads). The response of the system to an external bias voltage applied to it is the tunnelling current. One may learn about the charge and spin properties of strongly correlated electrons in the QD by means of measuring its conductance g as a function of temperature, applied bias, gate voltages and external magnetic field. One may also study the optical properties of QD, which are determined by the linear and non-linear response of QD at high frequencies. We are interested in manifestations of dynamical symmetry in these measurements. The pertinent properties of several types of quantum dots are discussed below.

2.1 Planar dots

A planar (lateral) quantum dot is formed in a 2D depletion layer on the interface between two semiconductors (usually, GaAs/$Ga_{1-x}Al_xAs$). The electrodes imposed on this structure form both the confining potential well (quantum dot) and the dot-lead junctions (Fig. 2). If the junction is narrow enough, a single electron mode connects the dot and the Fermi reservoirs of electrons in the "metallic" leads. The discrete energy spectrum of electrons in the confined region is characterized by single-particle levels ϵ_i with typical inter-level spacing $\delta\varepsilon$ and charging energy Q, which is predetermined by the capacitance C of the dot, namely, $Q = e^2/2C$. Typical values of the parameters characterizing planar quantum dots are $\delta\varepsilon \approx 100-150\mu eV$, $Q \approx 500-600\mu eV$, so the charging energy is large enough, and it predetermines the character of electron tunnelling through the dot.

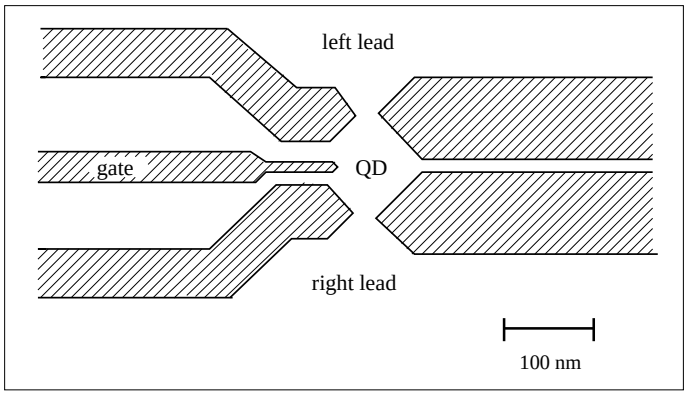

Figure 2: Planar quantum dot. Electrodes imposed on a semiconductor heterostructure are drawn schematically as shaded profiles.

Now one may schematically represent the energy spectrum of a planar quantum dot coupled by tunnel contacts to the leads in the following way: The discrete electron levels in the dot and the metallic electron continuum in the leads in an equilibrium state have the same chemical potential $\mu = \mu_L = \mu_R$, where the indices

L, R denote the electron liquid in the left and right lead, respectively (see Fig. 3a). However, tunnelling through planar quantum dots is blocked by the charging energy Q in the weak coupling limit, where the tunnelling rates $\gamma_{L,R}$ are the smallest energies compared with all other energy parameters characterizing electrons in the circuit,

$$\gamma_{L,R} \ll \delta\varepsilon < Q \ll D_{L,R}. \tag{16}$$

(here $D_{L,R}$ is the bandwidths characteristic for the kinetic energy of electrons in the leads). This is the familiar Coulomb blockade effect responsible for single electron tunnelling in nano-size devices [14]. The Coulomb blockade fixes the number of electrons $\mathcal{N}$ in planar quantum dots. In the neutral state of planar quantum dots the value of $\mathcal{N} = \mathcal{N}_0$ is determined by minimization of the total energy of the dot $\mathcal{E}(\mathcal{N})$. Then, injection of one more electron into the initially neutral dot costs an *addition energy* $\epsilon_{\mathcal{N}_0} = \mathcal{E}(\mathcal{N}_0 + 1) - \mathcal{E}(\mathcal{N}_0) - \mu$. This energy equals

$$\epsilon_{\mathcal{N}_0} = \begin{cases} Q - \mu & \text{for odd } \mathcal{N}_0 \\ \delta\varepsilon + Q - \mu & \text{for even } \mathcal{N}_0 \end{cases} \tag{17}$$

(see Fig. 3b,c). The planar quantum dot with odd occupation is characterized by its spin 1/2, whereas a dot with even occupation is generically in a singlet spin state due to the Pauli principle. It is clear from Eqs. (17), that electron tunnelling through planar quantum dots is possible only provided the additional energy vanishes. To achieve this resonance condition, a gate voltage v_g is applied to the dot, so that resonance tunnelling occurs when $\epsilon_{\mathcal{N}} - v_g = 0$. Then, increasing v_g one may reach the resonance conditions for $\epsilon_{\mathcal{N}}$ with $\mathcal{N} = \mathcal{N}_0 + 1,\ \mathcal{N}_0 + 2,\ \mathcal{N}_0 + 3$, etc. This is the mechanism of single electron tunnelling, which was realized in various devices manifesting Coulomb blockaded features [15].

Returning now to the dynamical symmetry aspect of this phenomenon, one should consider only the low-energy part of the electron spectrum in planar quantum dots, which is comparable with the energy scale characteristic for the interaction with the metallic reservoirs (electrons in the leads). This scale is determined by the tunnelling rates $\gamma_{L,R}$ and the energy $k_B T_0$ of more subtle many-particle effects, which will be specified below (k_B is the Boltzmann constant). As has been shown in the previous section, dynamical symmetries become essential when intrinsic or extrinsic level degeneracy exists in a nano-object. Having this in mind, one can ignore most states of planar quantum dots except the ground state with its energy $\mathcal{E}(\mathcal{N}_0)$ and those states which may enter the resonance under the influence of external fields (gate voltage, magnetic field, etc). In case of odd occupation, the only possibility is the Coulomb resonance determined by the condition $\epsilon_{\mathcal{N}_0} \approx (\gamma_{L,R},\ k_B T_0)$. Then only the following states,

$$\begin{aligned} E_\Lambda(\mathcal{N}_0) &= \varepsilon_d - v_g, \quad \Lambda = \sigma \\ E'_\Lambda(\mathcal{N}_0 + 1) &= 2(\varepsilon_d - v_g) + Q, \quad \Lambda' = S, \end{aligned} \tag{18}$$

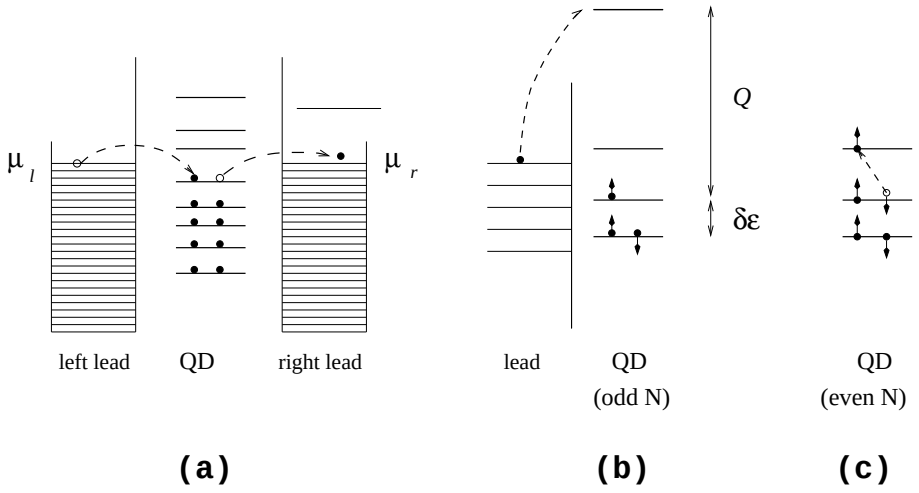

Figure 3: Energy levels for electrons in planar quantum dot. (a) General level scheme for odd $\mathcal{N}_0$; (b) Zoomed highest occupied states and lowest unoccupied states for odd $\mathcal{N}_0$; (c) Zoomed highest occupied states for even $\mathcal{N}_0$. Electron tunnelling processes between leads and QD (a),(b) and within QD (c) are shown by dashed arrows.

should be retained in the Hamiltonian (2). Here ε_d is the last occupied electron level in the dot. Thus, an accidental degeneracy is possible only between the states belonging to adjacent charge sectors $\mathcal{N} = (\mathcal{N}_0, \mathcal{N}_0 + 1)$.

A richer situation emerges for even occupation. In this case the Coulomb resonance is also possible, but there arises an additional possibility of dynamical processes within a given charge sector $\mathcal{N} = \mathcal{N}_0$. The energy states in this sector are

$$\begin{aligned} E_\Lambda(\mathcal{N}_0) &= 2(\varepsilon_d - v_g), \quad \Lambda = S \\ E_{\Lambda'}(\mathcal{N}_0) &= 2\varepsilon_d + \delta\varepsilon - 2v_g - J_d, \quad \Lambda = E_T, \\ E_{\Lambda''}(\mathcal{N}_0) &= 2\varepsilon_d + \delta\varepsilon - 2v_g, \quad \Lambda = E_S. \end{aligned} \tag{19}$$

The second and third levels above correspond to triplet and singlet excitonic states, where one of the electrons moves from the highest occupied level to the lowest empty level. The parameter J_d is the intra-dot exchange interaction responsible for the singlet/triplet level splitting. The symmetry of this manifold is $SO(5)$ according to the classification scheme given above. If not all these states are involved in the interaction with reservoir, the symmetry is effectively reduced. Several examples of symmetry reduction will be discussed below.

2.2 Vertical dots

Vertical dots have been fabricated in numerous experiments. The main feature of such device is that the geometrical symmetry of the dot (usually cylindrical) occurs also in the lead. This implies that electrons has, beside spin, an additional

quantum number which is attached to them wherever they are. Electrostatic confinement potential in vertical quantum dots with cylindrical symmetry can be approximated by a 2D harmonic potential. Such potential gives rise to shell structure of discrete electron states. Like in "natural" atoms, these states are classified as $1s,\ 2s,\ 2p,\ 3s,\ 3p,\ 3d...$ and electronic states are filled sequentially in accordance with Hund's rule. The occupation numbers corresponding to filled shells can be regarded as "magic numbers" $\bar{\mathcal{N}}$ with maximum addition energy $\Delta\mathcal{E}_{\bar{\mathcal{N}}}$. Indeed, the atom-like character of filling these artificial atoms with tunable number of electrons in the dot $0 \leq \mathcal{N} \leq 23$ was observed experimentally [16].

Like in the case of real atoms the structure of electron shells is predetermined by the single-particle quantum numbers and full orbital and spin momenta of electrons in the last partially filled shell. Having in mind possible manifestations of dynamical symmetry, we are especially interested in hidden and accidental degeneracies characterizing the electron spectrum of vertical dot. These features may be revealed already for non-interacting electrons in parabolic potential described by the Fock-Darwin equation [17]. In this case the electron levels are characterized by the main quantum number n, radial number $n_r = 1,\ 2,\ 3...$, z-component of angular momentum $m = 0,\ \pm 1,\ \pm 2...$ and spin projection $\sigma = \pm 1/2$. The degeneracy intrinsic to the spectrum is determined by the condition

$$n = 2n_r + |m| + 1, \tag{20}$$

whereas the discrete energy levels ϵ_n are determined by the law $\epsilon_n = n\hbar\omega_0$, where $\hbar\omega_0$ is the electrostatic confinement energy. Besides, the electrons in the vertical dot possess orbital diamagnetism, so that the energy spectrum in the presence of a magnetic field $\mathbf{B}$ applied along the cylindrical axis is split in accordance with the following equation

$$\epsilon_n(B) = (2n_r + |m| + 1)\hbar\sqrt{\frac{\omega_0^2}{4} + \omega_c^2} - \frac{m}{2}\hbar\omega_c\ , \tag{21}$$

where $\omega_c = eB/m^*c$ is the cyclotron frequency (the Zeeman splitting is negligibly small in comparison with diamagnetic shift in GaAs) . It follows from Eqs. (20) and (21) that (i) the magic numbers are $\bar{\mathcal{N}} = 2,\ 6,\ 12,\ 20$, etc, and (ii) that crossing of levels with different n_r, m at some values of magnetic field is feasible (see Fig. 4a).

The level crossing pattern becomes even more complicated when the electron-electron interaction is taken into account [18]. In the simplest case of $\bar{\mathcal{N}} = 2$ the two-electron states are characterized by the total spin S and total orbital momentum M. At zero magnetic field the ground state is singlet ${}^2S:\ (S = 0, M = 1)$ and the excited state is triplet ${}^1T:\ (S = 1, M = 0)$. These levels cross at certain $B = B_c$ (Fig. 4b), and the effective symmetry of the vertical dot is $SO(4)$ in the vicinity of level crossing. When the second shell is partially filled ($\mathcal{N} = 3, 4, 5$) more than two multiplets are involved in the level crossing pattern [19], so that the dynamical symmetry becomes really complicated.

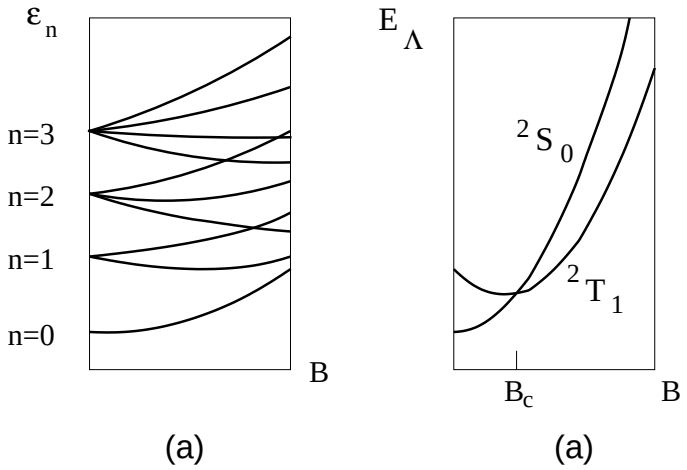

Figure 4: Energy levels for electrons in vertical quantum dot. (a) single electron energy levels [see Eq. (21)]; (b) two-electron singlet and triplet energy levels.

2.3 Semiconductor nanoclusters

Semiconductor nanocrystals prepared by means of colloidal chemistry methods [8] and self-assembled dots grown as islands in strained lattice-mismatched films [9] have regular geometrical shapes and conserve the bulk crystal structure. As a result, the discrete electron spectrum in these nanoclusters retains many feature of Kane electron-hole spectrum of bulk III-V or II-VI semiconductors [20]: the characteristic energy is in the eV scale, the same as in bulk materials. The nomenclature of discrete highest occupied states in the valence band and lowest unoccupied states in the conduction band is inherited from the *sp*-hybrid states in the vicinity of the Γ point of the 3D Brillouin zone.

The excitonic spectrum of these nanoclusters is of primary interest. Single exciton lines due to interband excitations are observed in optical and tunnel spectra [21]. High-excitation spectroscopy methods allow experimental observation of exciton complexes [22] and even exciton droplets [23] in arrays of self-assembled dots. These multiexciton levels may be degenerate due to geometrical and dynamical symmetries.

The idea of hidden symmetry of excitonic states in quantum dots [24] is borrowed from the theory of excitons in 2D electron gas in an Integer Quantum Hall Effect regime [25]. The algebra of exciton operators is predetermined by the special properties of Coulomb interaction for this two-component Fermi liquid. These

operators form a vector $\mathbf{P}$ with the following spherical components:

$$P^+ = \sum_i e^\dagger_{p\sigma} h^\dagger_{p,-\sigma},\ P^- = \sum_p h_{p,-\sigma} e_{p\sigma},\ P_z = \frac{1}{2}\left((N^e_\sigma + N^h_\sigma) - N_{tot}\right). \qquad (22)$$

Here $e^\dagger_{p\sigma},\ h^\dagger_{p,-\sigma}$ are, respectively, creation operators for the electron and hole with respective single-particle energies $E^{(e,h)}_p$. The operators $P^\pm$ create/annihilate an exciton, and the operator P_z measure the population inversion on a shell with orbital degeneracy N_{tot}. In terms of dynamical symmetry, these operators describe transitions from the ground state (with zero energy) to a single exciton state. In accordance with Eq. (6) these operators do not commute with the electron-hole Hamiltonian $\mathcal{H}_{eh}$, which includes the single particle term and the Coulomb interaction $\langle pq|V|rs\rangle$, where $\{pqrs\}$ are various hole and electron states on a given shell of the QD. Quite unexpectedly, the commutation relation (6) reads in this case

$$[P^+, \mathcal{H}_{eh}] = -E_0 \mathcal{H}_{ex}, \qquad (23)$$

where $E_0 = E^{(e)}_p + E^{(h)}_p$ is the energy of an electron-hole pair. All Coulomb contributions cancel each other exactly. This cancellation is a consequence of hidden symmetry of Coulomb interaction in quantized two-component Fermi system: interactions between particles of the same kind coincide with each other and (with reversed sign) with that of different kinds. It follows from this property that creation of n excitons of the same kind described by the operator $(P^+)^n$ costs an energy nE_0. This enables a strong degeneracy of the multi-exciton spectra: for example, the energy level of biexciton is twice the energy of a single exciton, etc. Of course, any small perturbation removes the degeneracy between a singlet-singlet and triplet-triplet states of a biexciton, but the dynamical symmetry still exists.

2.4 Complex quantum dots

The isolated quantum dots considered above are typical examples of artificial atoms. A double valley quantum dot with weak capacitive and/or tunnelling coupling between its two wells may be considered as a simplest case of artificial molecule. Such double quantum dots (DQD) were fabricated several years ago [13]. Two wells in DQD may be identical or have different size; the DQD may be integrated within an electric circuit either in series or in parallel; different gate voltages may be applied to each well. Moreover, one of the two wells may be disconnected from the leads (side geometry). All these configurations are presented in Fig. 5. Vertical quantum dots also may form a DQD. Such a variety of configurations promises even more possibilities for manifestations of dynamical symmetry effects in artificial molecules than in artificial atoms.

Let us consider the electron spectra of DQDs shown in Fig. 5 [26]. In Section I we discussed dynamical symmetries of hydrogen-like systems (H^0, $H^\pm$ states of

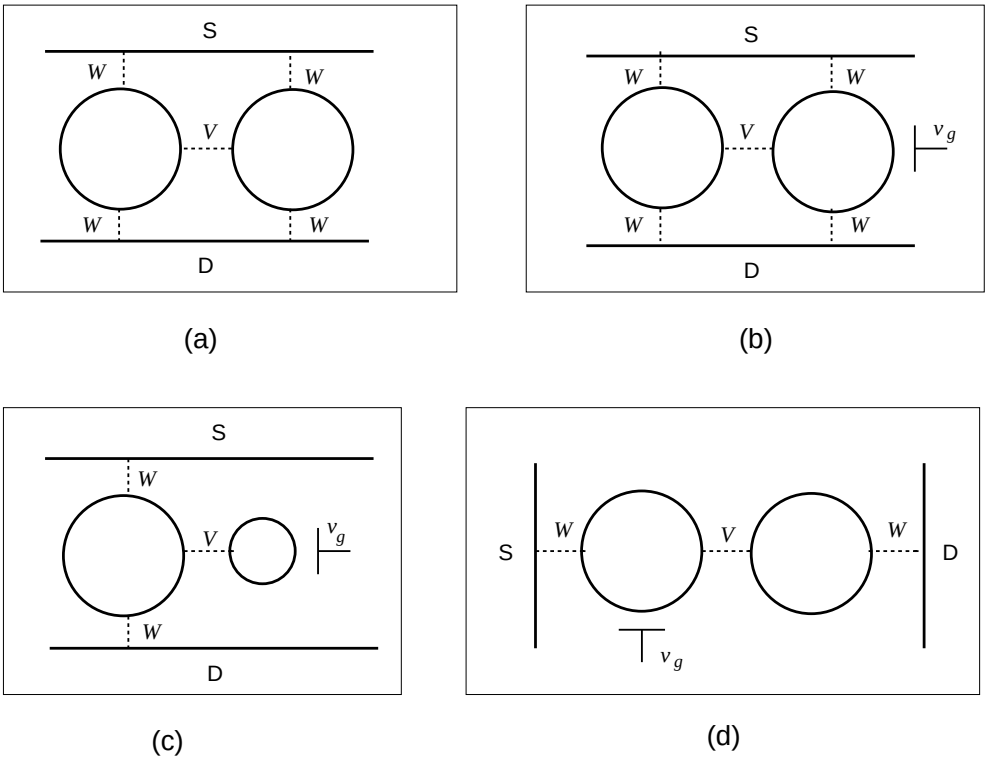

Figure 5: Various types of double quantum dots (DQD). Tunnelling channels are marked by dashed lines, V and W are tunnelling constants. (a) Symmetric DQD in parallel geometry; (b) biased symmetric DQD in parallel geometry; (c) asymmetric DQD in side (T-shaped) geometry; (d) DQD in series geometry.

atomic hydrogen). It is clear that the symmetric DQD shown in Fig. 5a has the main features of hydrogen molecule H_2 and molecular ions $H_2^{\pm}$ for the occupation number $\mathcal{N} = 2, 1, 3$, respectively. To exploit this analogy, we assume that the neutral state of DQD corresponds to $\mathcal{N} = 2$, and each valley is also neutral when occupied by a single electron, $\mathcal{N}_i = 1, i = l, r$. Then two valleys are coupled only by tunnel channel, and in case of strong Coulomb blockade in each valley, $Q \gg V$ (V is a tunnelling constant), the system is an analog of H_2 in the Heitler-London limit. If the two valleys are completely identical, the spectrum E_Λ consists of two low-lying spin states $E_{S,T}$ and two charge transfer excitons $E_{e,o}$ (even singlet and odd triplet), with

$$\begin{aligned} E_S &= 2\varepsilon - 2V\beta, \quad E_T = 2\varepsilon \\ E_o &= 2\varepsilon + Q, \quad E_e = 2\varepsilon + Q + 2\beta V \ . \end{aligned} \tag{24}$$

Here $\varepsilon = \varepsilon_l = \varepsilon_r$ are the one-electron levels. The spectrum is calculated under the assumption $\beta = V/Q \ll 1$. The origin of a narrow spin gap $\sim \beta V$ and a wide charge

transfer gap $\sim Q$ in the two-electron spectrum is inter-valley tunnelling, which is possible only in singlet configurations. Fig. 6a illustrates this mechanism.

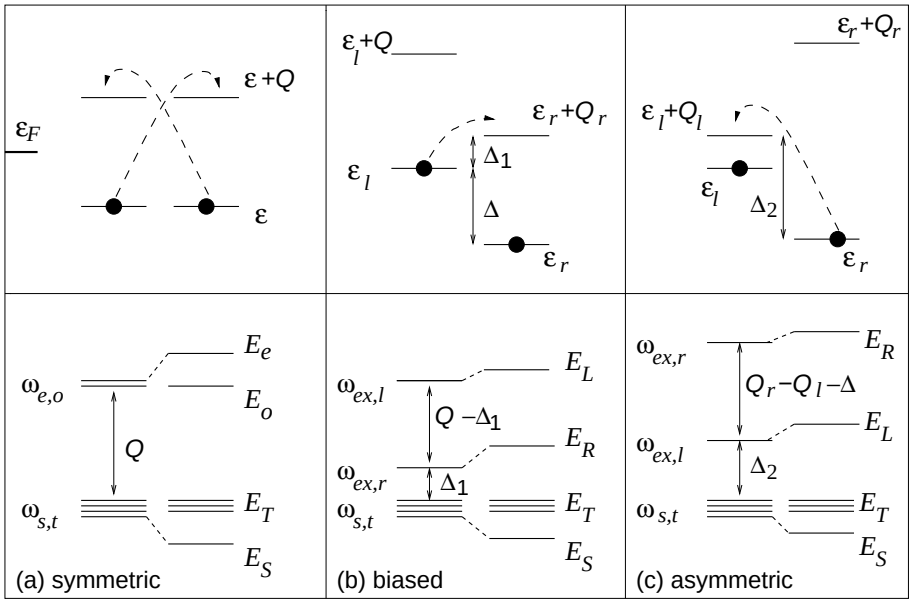

Figure 6: Energy level schemes for symmetric, biased and asymmetric DQD. Upper panels: single electron levels. Tunnel processes responsible for formation of charge transfer excitons are shown by dashed lines. Lower panels: degenerate two-electron energy levels ω_α without interwell tunnelling V and split two-electron levels E_Λ renormalized by interwell tunnelling in second order.

One may break the left-right symmetry by means of an external gate voltage difference $v_{gl} - v_{gr}$ applied to the DQD configuration (Fig. 5b). This voltage can be tuned in such a way that one of two charge transfer excitons becomes "soft" enough to influence the low-lying spin excitations (Fig. 6b). In this case, only three levels should be taken into account when discussing the dynamical symmetry: these are the same singlet and triplet states plus a singlet charge-transfer exciton ("right" exciton in the geometry illustrated by Fig. 6b. The corresponding energy levels are

$$\begin{aligned} E_S &= \varepsilon_l + \varepsilon_r - 2\beta_1 V, \quad E_T = \varepsilon_l + \varepsilon_r, \\ E_R &= 2\varepsilon_r + Q + 2\beta_1 V \ . \end{aligned} \tag{25}$$

Finally, the two constituents of a DQD may have different size (Fig. 5c). We discuss this case in a side geometry, where the right dot of a smaller size R_r is disconnected from the leads.

If $R_r \ll R_l$, then $Q_r \gg Q_l$, and the relevant part of the spectrum of doubly

occupied DQD shown in Fig. 6c is

$$\begin{aligned} E_S &= \varepsilon_l + \varepsilon_r - 2\beta_2 V, \quad E_T = \varepsilon_l + \varepsilon_r, \\ E_L &= 2\varepsilon_l + Q_l + 2\beta_2, \end{aligned} \tag{26}$$

In this case the "right" charge transfer exciton is retained in the manifold.

It follows from the above analysis, that DQD may manifest $SO(3)$, $SO(4)$ or $SO(5)$ dynamical symmetries depending on the relevant physical processes, in which the DQD is involved. The first of these symmetries is simply a symmetry of a spin $S = 1$, while in the second case, both spin singlet and spin triplet are involved. In the third case, the charge transfer exciton also plays its part. All these situations will be discussed in subsequent sections.

Next, the symmetry of a DQD with $\mathcal{N} = 1$ should be exposed. Again, we consider the case of strong Coulomb blockades in both valleys, where the doubly occupied states are eliminated. Although this restriction sounds rather formal in the case of single electron occupation, it starts to play an essential role when the interaction with the reservoir is switched on. The dynamical symmetry of this system was analyzed in [27]. We restrict ourselves to the case of symmetric or nearly symmetric DQD in a series geometry (Fig. 5d). If $\varepsilon_l \approx \varepsilon_r$, then four states have approximately the same energy, namely left or right dot occupied by an electron with spin projection $\uparrow$ or $\downarrow$. One may introduce a pseudospin $T_z = (\mathcal{N}_l - \mathcal{N}_r)/2 = \pm 1/2$, which describes the electron configuration in the DQD. Denoting the two components of this pseudospin states as $\pm$, one may construct a "hyperspin" χ_4 including all four states

$$\chi_4 = \{+\uparrow, +\downarrow, -\uparrow, -\downarrow\}. \tag{27}$$

This spinor transforms in accordance with representations of the $SU(4)$ group. If the four-fold degeneracy of the DQD is violated by external fields (gate voltage or magnetic field), the remaining symmetry is $SU(2)$. In particular, one may imagine the situation when only the pseudospin $\mathbf{T}$ is involved in the dynamical symmetry, and spin variable plays part of "flavor" [28, 29]. The case of a symmetric DQD with $\mathcal{N} = 3$ may be considered similarly because of particle-hole and spin up-spin down symmetry of the nano-object.

Another way to obtain an artificial molecule is to fabricate two vertically stacked columnar quantum dots coupled by tunnelling interaction [30]. Of course, the familiar singlet/triplet level crossing induced by diamagnetic level shift is expected for a H_2-like molecule with $\mathcal{N} = 2$ [31]. More complex molecular spectra appear at higher occupations $\mathcal{N} > 2$. An especially exotic state such as a "bipolar" molecule arises when two vertically stacked quantum dots are populated by carriers of different kinds – electrons and holes [32].

Recently it was shown that even richer picture of dynamical symmetries may arise in triple quantum dots (TQD) with $\mathcal{N} = 4$ both in parallel and sequential geometries [33]. In addition to the situation of nearly degenerate singlet-singlet-triplet manifold ($SO(5)$ symmetry) the triplet-triplet-singlet level crossing can occur

in TQD under certain conditions. The dynamical symmetry of this manifold is $SO(7)$. Following the arguments of Ref. [27], it is clear that the same TQD with $\mathcal{N} = 1$ should possess $SU(6)$ symmetry.

To conclude, the notion of dynamical symmetries is the natural language, which is extremely useful in the description of quantum dots. These nano-objects possess a plethora of dynamical symmetries, which may be unveiled due to interaction with metallic reservoirs and external fields. Various physical realizations of these dynamical symmetries will be described in subsequent sections.

3 Dynamical symmetries broken by interaction with reservoir

As long as the dot is isolated from its environment, it conserves the symmetry related to its spin state, charge state and as well as its geometrical symmetry. In a simple case when only spin and charge are conserved quantities, the generic Hamiltonian of an isolated QD may be written in terms of these conserved quantities

$$\mathcal{H}_{dot} = \sum_{i\sigma} \epsilon_i n_{i\sigma} + Q(\mathcal{N} - \mathcal{N}_0)^2 - J\mathbf{S}^2. \tag{28}$$

Here the first term describes the discrete spectrum of the QD and the two other terms stem from electrostatic and exchange interactions and describe the Coulomb blockade of charge states (deviating from the neutral state with $\mathcal{N} = \mathcal{N}_0$) and the total spin of the dot. A tunnelling contact with reservoir may break the symmetry of $\mathcal{H}_0$ and, hence, violate spin and charge conservation. The global spin and charge in a system as a whole is conserved, but interaction with environment can change both these quantities in the dot. The simplest example of interaction, which changes the charge in the dot is electron tunnelling between the dot and the electronic reservoir, and the simplest spin-dependent interaction is that of direct exchange between the dot and the lead electrons.

We discuss first the tunnelling contact. The basic tunnel Hamiltonian is

$$\mathcal{H}_{tun} = \sum_{\alpha k i\sigma} W^{i\sigma}_{\alpha k} \left(c^{\dagger}_{\alpha k\sigma} d_{i\sigma} + H.c. \right). \tag{29}$$

Here $W^{i\sigma}_{\alpha k}$ is the tunnel matrix element, $d_{i\sigma}$ is the operator destroying the dot electron in the level iϵ_i and $c^{\dagger}_{\alpha k\sigma}$ is the operator creating an electron in the lead α of metallic reservoir described by the Hamiltonian

$$\mathcal{H}_{band} = \sum_{\alpha=l,r} \sum_{k\sigma} \varepsilon_{\alpha k\sigma} c^{\dagger}_{\alpha k\sigma} c_{\alpha k\sigma}. \tag{30}$$

Below we discuss the case of weak tunnelling, where the QD is connected only by one tunnelling channel with each lead and the inequalities

$$W^{i\sigma}_{\alpha k} \ll \delta\epsilon_i \ll Q \tag{31}$$

are valid. In this case only the highest occupied levels of QD are involved in tunnelling, and the energy cost of single electron tunnelling between the lead and the QD is

$$E_{\pm} = \begin{cases} \epsilon_{\mathcal{N}+1} - \varepsilon_{\alpha k\sigma}, & k < k_F \\ \varepsilon_{\alpha k\sigma} - \epsilon_{\mathcal{N}}, & k > k_F \end{cases}$$

Here $\epsilon_{\mathcal{N}+1} = E_{\Lambda'}(\mathcal{N}_0+1) - E_{\Lambda}(\mathcal{N}_0)$ and $\epsilon_{\mathcal{N}} = E_{\Lambda}(\mathcal{N}_0) - E_{\Lambda'}(\mathcal{N}_0-1)$ are electron addition and extraction energies respectively, and k_F is the Fermi momentum of electrons in the lead [cf. Eqs. (17) – (19)].

It is convenient to rewrite $\mathcal{H}_{tun}$ in terms of Hubbard operators:

$$\mathcal{H}_{tun} = \sum_{\alpha k\sigma} \left[\sum_{\Lambda\lambda} \left(W^{\Lambda\lambda}_{\alpha k} X^{\Lambda\lambda} c_{\alpha k\sigma} + H.c. \right) + \sum_{\Lambda\gamma} \left(W^{\gamma\Lambda}_{\alpha k} X^{\gamma\Lambda} c_{\alpha k\sigma} + H.c. \right) \right] \tag{32}$$

Here the states from the charge sectors $\mathcal{N}_0 \mp 1$ are denoted by indices λ and γ, respectively. If the gate voltages are tuned so that either an addition or extraction energy is zero, we are at resonance and tunnelling through the dot is possible. The dot then becomes "transparent" in accordance with the Breit-Wigner formula for transmission coefficient $\mathcal{T}(\varepsilon)$:

$$\mathcal{T}(\varepsilon) = \frac{\Gamma_l \Gamma_r}{[\varepsilon - E_{\pm}(k_F)]^2 + (\Gamma_l + \Gamma_r)^2/4}, \tag{33}$$

where $\Gamma_\alpha = \pi \rho_{0\alpha} |W^{\pm}_{\alpha}|^2$ are the tunnelling rates for the left and right lead, $\rho_{0\alpha}$ is the density of electron states on the Fermi level of the lead α, $W^{\pm}_{\alpha}$ are the matrix elements for addition/extraction tunnelling taken from the Hamiltonian (32). These processes are responsible for single-electron tunnelling through quantum dots, which results if the ubiquitous Coulomb staircase for the current-voltage characteristics prevails. This form of single electron transistor arises in tunnel junctions and, as far as the tunnelling current is concerned, serves as a replacement of the Ohm's law [15].

The second order tunnelling processes described above cannot reveal any dynamical symmetry of QD because they do not change the state of the dot (see Fig. 7a). On the other hand, dynamical symmetries can be exposed by *cotunnelling* processes out of resonance (on the Fermi level) (Fig. 7b): in the first step of a two-stage cotunnelling process an electron from the occupied level ϵ_1 leaves the dot and then, in the second step, an electron from the same or another lead replaces it in the empty level ϵ_2. The many-electron state of a QD changes from Λ_1 to Λ_2, and if the operator $X^{\Lambda_2\Lambda_1}$ belongs to a set of generators of a dynamical group, this *inelastic* cotunnelling may be described by means of the group theoretical manipulations introduced above.

The effective vertex Γ for this inelastic cotunnelling has the form

$$\Gamma^{\Lambda_1\Lambda_2}_{\alpha k\sigma,\alpha' k'\sigma'}(\varepsilon) \sim \frac{W_\alpha W_{\alpha'}}{(\varepsilon - \delta\epsilon)} c^{\dagger}_{\alpha k\sigma} c_{\alpha' k'\sigma'} X^{\Lambda_2\Lambda_1} \tag{34}$$

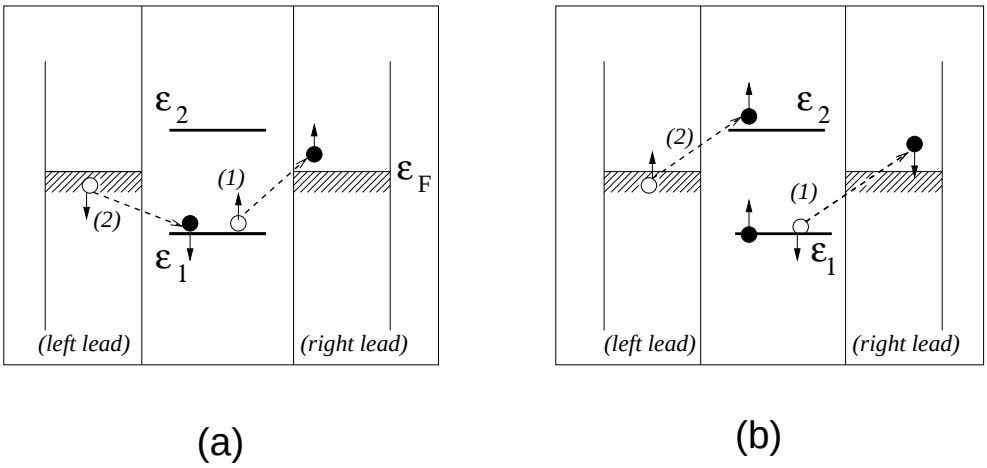

Figure 7: Cotunneling through planar QD with odd (a) and even (b) occupation.

Here $\delta\epsilon$ is the additional energy of the dot in the process of two-stage cotunnelling.

The fact that cotunnelling process is accompanied by spin reversal, $\sigma \neq \sigma'$ is crucial. At the bottom line it means that this two-particle process may be treated also as an effective exchange, which involves the dot particles and electrons from both leads. In a situation where the system is set away from a Coulomb resonance, $E_{\pm}(k_F) \gg W_\alpha$, the only process, which survives is this indirect exchange (in its full quantum-mechanical sense), where only the electron residing on the highest occupied level ϵ_h of the dot is involved in cotunnelling. Then $\delta\epsilon = Q$, and the vertex Γ combines with direct exchange between the dot and lead electrons to generate the effective spin Hamiltonian for *an elastic* cotunnelling

$$\mathcal{H}_{cot} = \sum_{\alpha\alpha'} \sum_{kk'} J_{\alpha\alpha'} \mathbf{S} \cdot \mathbf{s}_{\alpha k, \alpha' k'}. \tag{35}$$

with $J_{\alpha\alpha'} = \Gamma^0_{\alpha k_F, \alpha' k'_F}(0)$ Here the upper index '0' indicate that only the spin state of the dot is changed in the course of cotunnelling.

The Hamiltonian (35) has the form of the well known Kondo Hamiltonian, which was introduced in order to explain the anomalous shallow minimum in the resistance of metals doped be magnetic impurities. This analogy between magnetic scattering in bulk metal and magnetic tunnelling through insulating barrier was noticed in the mid 60ies [34]. Later on, this idea was extended to the physics of tunnelling through nano-objects such as quantum dots [35]. For quite a number of years now, resonance Kondo tunnelling is at the focus of contemporary physics of quantum dots and related objects (such as carbon nanotubes or organometallic complexes). There are several reasons for this exceptional interest. First, the Kondo effect *per se* is a complex many-particle phenomenon, which can be formulated in terms of integrable 1D problem (using e.g Bethe Ansatz). Second, Kondo tunnelling manifests itself

as an enhanced quasi elastic resonance, and thus, it can be detected as a zero bias anomaly (ZBA) in a tunnelling conductance away from Coulomb resonance peaks in the so called Coulomb windows which form a diamond-shape lattice of valleys in the plane (v_b, v_g) [15]. (here v_b and v_g are external bias and gate voltage, respectively). These zero-bias anomalies were detected in planar QD in the late 90ies [36]. Thereafter, similar effects were found in nanotubes [38] and vertical dots [37, 39]. In the two latter cases, the anomalies related to the the $SO(4)$ dynamical symmetry in Kondo tunnelling were noticed for the first time.

3.1 Dynamical symmetry in Kondo cotunnelling

Prima facie, the cotunneling Hamiltonian (35) in conjunction with the Hamiltonian (28) for the isolated QD leaves no room for manifestations of dynamical symmetry. The only operator characterizing the excitations in the QD which are involved in the interaction with reservoirs is the spin $\mathbf{S}$. This exchange interaction, of the form $J\mathbf{s}\cdot\mathbf{S}$ breaks the $SU(2)$ symmetry of the QD, and the multiple creation of electron-hole pairs with spin reversal results in the formation of a singlet ground state in case when the spin of the dot is $S = 1/2$ [35]. This situation is realized in QD with odd occupation number (see Fig. 3b). Indeed in the first experiments [36], Kondo-type ZBA were observed only in Coulomb windows with odd $\mathcal{N}$. Soon after, though, theoretical predictions about possible realizations of Kondo mechanism of cotunneling in QD with even $\mathcal{N}$ in external magnetic field were reported [40, 41, 42]. They were promptly verified experimentally [38, 39]. Later on, possible occurrence of Kondo effect in evenly occupied double quantum dots without magnetic field assistance was suggested [26].

Most of theoretical investigations pertaining to even $\mathcal{N}$ appealed implicitly or explicitly to the concept of dynamical symmetry of the QD, which was discussed in Section II. The simplest case of even occupation is $\mathcal{N} = 2$ of course. This situation may be easily realized in planar QD (see Section II.A), vertical QD (Section II.B) and double QD (Section II.D). Let us recall that in case of odd $\mathcal{N}$ where there is a single electron in the highest occupied level of QD, its spin may be reversed due to cotunneling together with creation of electron-hole pair, thus resulting in the effective Hamiltonian (35). A similar process may result in a singlet-triplet transition in case of two electrons in the highest occupied level. Thus the vector operator $\mathbf{R}$ describing these singlet-triplet transitions (7) enters the effective Hamiltonian together with the spin vector operator $\mathbf{S}$:

$$\mathcal{H}_{cot} = \sum_{\alpha\alpha'}\sum_{kk'}\left(J^{(1)}_{\alpha\alpha'}\mathbf{S}\cdot\mathbf{s}_{\alpha k,\alpha' k'} + J^{(2)}_{\alpha\alpha'}\mathbf{R}\cdot\mathbf{s}_{\alpha k,\alpha' k'}\right). \tag{36}$$

One should remember, however, that in all cases mentioned above the ground state of the isolated QD is singlet. The energy gap $\Delta_s = E_T - E_S$ between the

triplet and singlet levels is

$$\Delta_s = \begin{cases} \delta\varepsilon - J_d & \text{in planar QD} \\ J_d & \text{in vertical QD} \\ 2\beta V & \text{in double QD} \end{cases} \tag{37}$$

[see Eqs.(19)) and (24)]. The Kondo effect is characterized by the energy scale E_K (Kondo energy), which is exponentially small: in the simple case described by the Hamiltonian (35),

$$E_K = k_B T_K \sim D_0 \exp(-1/\rho_0 J_{max}), \tag{38}$$

where J_{max} is the maximum of all coupling constants entering this Hamiltonian and D_0 is the effective energy band width for the electrons in the leads. If $\Delta_s \gg E_K$ Kondo screening is ineffective and no ZBA in the conductance develops. In accordance with general principles described in Section I, the dynamical symmetry enters the physical considerations provided $\Delta_s \sim E_K$, so the special mechanisms compensating the spin gap Δ_s should exist to allow Kondo screening in quantum dots with even occupation. Such mechanisms exist in all three systems under discussion. A concrete description of *singlet-triplet crossover* in QDs is given below.

Let us start with vertical dots, where the mechanism of singlet-triplet crossover is simple from a theoretical point of view and may be easily realized experimentally. As was mentioned in Section II.B, the occasional singlet-triplet degeneracy arises due to diamagnetic shift of single electron levels in an external magnetic field (Fig. 4b). To derive the effective spin Hamiltonian, one should start with the Anderson Hamiltonian

$$\mathcal{H}_A = \mathcal{H}_{dot} + \mathcal{H}_{band} + \mathcal{H}_{tun}, \tag{39}$$

where the approximation (28) is *not enough* even for adequate description of the charge sector $\mathcal{N} = 2$, in which the states $\{\Lambda = S, T\mu\}$ from the singlet/triplet manifold should be included. In terms of the group generators this term in the Anderson Hamiltonian may be rewritten as

$$\mathcal{H}_{dot} = \frac{1}{2}\left(E_T \mathbf{S}^2 + E_S \mathbf{R}^2\right) + Q(\hat{\mathcal{N}} - 2)^2. \tag{40}$$

Besides, states from adjacent charge sectors, $\{\lambda, \gamma\}$ which are admixed due to the interaction $\mathcal{H}_{tun}$ (32) should be taken into account. Projecting out the virtual transitions to charge states with $\mathcal{N} = 1, 3$ by means of second order perturbation theory [43] or by employing the Schrieffer-Wolff (SW) canonical transformation [44] (which eliminates $\mathcal{H}_{tun}$), one maps the initial problem onto a reduced Fock space with conserved $\mathcal{N} = 2$. Before performing the SW transformation, it is worthwhile, in many cases, to execute a rotation in the lead Hamiltonian

$$\begin{aligned} c_{lk\sigma} &= c_{1k\sigma}\cos\vartheta_{k\sigma} + c_{2k\sigma}\sin\vartheta_{k\sigma} \\ c_{rk\sigma} &= -c_{1k\sigma}\sin\vartheta_{k\sigma} + c_{2k\sigma}\cos\vartheta_{k\sigma} \end{aligned} \tag{41}$$

with

$$\vartheta_{k\sigma} = \arcsin\left(W^{\sigma}_{lk}/\sqrt{|W^{\sigma}_{lk}|^2 + |W^{\sigma}_{rk}|^2}\right)$$

By this transformation the odd combination $c_{2k\sigma}$ is eliminated from the tunnel Hamiltonian [35], and eventually one arrives at the Hamiltonian (36) with diagonal coupling constants

$$\mathcal{H}_{cot} = \sum_{kk'}\left(J^{(1)}\mathbf{S}\cdot\mathbf{s}_{kk'} + J^{(2)}\mathbf{R}\cdot\mathbf{s}_{kk'}\right). \tag{42}$$

At this stage, the cotunneling problem can be approached by standard methods of the theory of Kondo scattering generalized to the case of $SO(4)$ symmetry, where the "scatterer" is described by a six-dimensional vector $\{\mathbf{S},\mathbf{R}\}$ instead of the usual $SO(3)$ vector $\mathbf{S}$ for spin 1.

The conventional Kondo problem [43, 45] is easily manageable at high temperatures $T > T_K$, where perturbation theory may be constructed by using the dimensionless quantity $j(\varepsilon)$,

$$j(\varepsilon) = \rho_0 J \ln(D_0/\varepsilon), \tag{43}$$

as a small parameter. This approach works until the current energy parameter ε is big enough to keep $j(\varepsilon) \ll 1$. The energy E_K defined by the equality $j(E_K) = 1$ is defined as the Kondo energy mentioned above as a characteristic energy of the Kondo problem. The crossover from the weak Kondo coupling to the strong coupling regime occurs around $\varepsilon \approx E_K$ [see Eq. (38)].

Summation of complicated perturbation series can be carried out by using the parquet equation technique [46], but one also may elegantly pack the same series in the solution of scaling equations within renormalization group (RG) theory [43, 47, 48, 49, 50] due to occurrence of logarithmic terms in the effective vertex which indicates that all energy scales in the Kondo problem are of equal importance. According to the RG scheme, one investigates the evolution of vertices and pertinent propagators by reducing the energy scale D (the bandwidth of the conduction electrons) in the Hamiltonian $\mathcal{H}_{band} + \mathcal{H}_{cot}$ from the bare bandwidth $D = D_0$ to the limiting value of $D \sim E_K$. The resulting low-energy spectrum is universal, which means that there exists a single energy scale E_K for all thermodynamic and dynamic variables.

If one employs Eq. (35) for the cotunneling Hamiltonian, the scaling flow trajectories are determined by a single equation for the effective dimensionless exchange vertex $\mathcal{J}(D)$

$$d\mathcal{J}/dL = -\mathcal{J}^2, \tag{44}$$

which should be solved with initial condition $\mathcal{J}(D_0) = \rho_0 J$. The solution is then,

$$\mathcal{J}(D) = \frac{\rho_0 J}{1 - j(D)}, \tag{45}$$

which implies that the effective coupling strength flows toward infinity when $D \to E_K$ or, in a temperature scale, $\mathcal{J}(T) = 1/\ln(T/T_K)$. This *stable infinite fixed point* determines the universality class of the Kondo problem. The scaling flow trajectory is trivial in this case: it is simply a ray (half line) emanating from the point $\mathcal{J}(D) = \rho_0 J$ and flowing to ∞. The RG approach cannot describe the subtle behavior of the system at $T \to 0$, but it encodes generic feature of Kondo cotunneling, i.e. formation of ZBA in Kondo regime. In the weak coupling regime $T > T_K$ the formation of the ZBA in tunnel conductance $g = dI/dV_b,\ V_b \to 0$ follows the scaling form [52]

$$g(T)/g_0 \sim \ln^{-2}(T/T_K), \tag{46}$$

where

$$g_0 = \frac{2e^2}{h}\frac{4\Gamma_l\Gamma_r}{(\Gamma_l+\Gamma_r)^2},$$

is the resonance conductance of the quantum dot (see Eq. 33). More sophisticated calculations at $T < T_K$ [53] allow one to describe the appearance of "Abrikosov-Suhl resonance" on the Fermi level ε_F responsible for the unitarity limit for the transmission coefficient $\mathcal{T}(\varepsilon \to \varepsilon_F)$.

The situation with the RG flow diagram for a QD possessing dynamical symmetry is more complicated. Since the Hamiltonian (42) contains two effective vertices, one gets a system of scaling equations [26, 42]

$$\begin{aligned} d\mathcal{J}_1/dL &= -[(\mathcal{J}_1)^2 + (\mathcal{J}_2)^2], \\ d\mathcal{J}_2/dL &= -2\mathcal{J}_1\mathcal{J}_2. \end{aligned} \tag{47}$$

The vertex $\mathcal{J}_2$ describes effective exchange due to S/T transitions, which are generically inelastic, because one has to absorb or release the energy of exchange splitting Δ_s to excite the singlet state in a situation when the ground state is a triplet ($\Delta_s < 0$). The scaling procedure for $\mathcal{J}_2$ stops at $D \sim |\Delta_s|$ and below this energy, only $\mathcal{J}_1$ continues to grow with decreasing D. Due to this effect the Kondo tunnelling is no more universal: unlike the conventional Kondo effect, it is impossible to draw the family of flow scaling diagrams in the plane $\{\mathcal{J}_1, \mathcal{J}_2\}$. The flow trajectory for $\mathcal{J}_1(D)$ still ends at stable infinite fixed point, but $\mathcal{J}_2$ is quenched at an intermediate energy, so the Kondo temperature becomes a function of Δ_s, which characterizes this quenching. Since one can change Δ_s in vertical QD by varying the magnetic field (see Fig.4b), one may reach the point of accidental degeneracy $\Delta_s = 0$ and change its sign. It is easily seen that T_K has maximum at $\Delta_s = 0$. In this case the system (47) reduces to a single equation (44) for the effective vertex $\mathcal{J}^+ = \mathcal{J}_1 + \mathcal{J}_2$. The corresponding Kondo temperature is

$$T_{K0} = D_0 \exp\left[-1/\rho_0(J_1 + J_2)\right]. \tag{48}$$

At finite $|\Delta_s|$ the Kondo temperature decreases and at $|\Delta_s| \gg T_{K0}$ it obeys a kind of universal law

$$T_K/T_{K0} = (T_{K0}/\Delta_s)^{\zeta}, \tag{49}$$

where $\zeta \lesssim 1$ is a numerical constant specific for a given type of QD [26, 42, 54].

Unlike the case of vertical dots, the singlet/triplet crossover in planar dots and double dots with even $\mathcal{N}$ may be achieved without the application of an external magnetic field due to somewhat rich and complicated structure of the low-energy states in an isolated QD. The most important fact is that the tunnelling amplitudes $W^{\Lambda\lambda}$ in the Hamiltonian (32) may be different for singlet ($\Lambda\lambda = S\bar{\sigma}$) and triplet ($\Lambda\lambda = T\sigma$) states. In planar QD the origin of this distinction is that electrons from *different* single electron states ϵ_1 and ϵ_2 are involved in the formation of S and T states, respectively (see Fig. 7b). Besides, one should remember that the singlet exciton also enters the manifold of low energy states [see Eq. (19)]. Although this manifold obeys $SO(5)$ dynamical symmetry, transitions to the highest singlet excitonic state does not enter explicitly into the set of dynamical variables involved in Kondo cotunneling. However the virtual transitions to this state may also influence the properties of S/T pair.

This situation is especially important for tunnelling through DQD with $\mathcal{N} = 2$ (see [26]). In this case the wave functions of electrons in S and T states are different because the intradot tunnelling V intermixes two singlet states [E_S and E_R in Eq. (25), E_S and E_L in Eq. (26)], while the triplet E_T is not affected by this process. As a result, a difference in tunnelling rates arises like in the case of planar QD, but in this case the sign of the difference is strictly determined, namely $W^{T\sigma} > W^{S\bar{\sigma}}$.

In a generic situation, one starts from the original Anderson Hamiltonian (40), (30), (32) and then arrives at the renormalized Kondo Hamiltonian (42) with effective vertices $\mathcal{J}_1, \mathcal{J}_2$ by two steps [51]. First, one has to take into account renormalization of the bare energies E_Λ in $\mathcal{H}_{dot}$ due to reduction of the energy scale $D_0 \to D$. This reduction is governed by the scaling equations

$$dE_\Lambda/dL = -\Gamma_\Lambda/\pi D. \tag{50}$$

The scaling trajectory for $E_\Lambda(D)$ is determined by a scaling invariant [43, 51]

$$E^*_\Lambda = E_\Lambda(D) - \pi^{-1}\Gamma_\Lambda \ln(\pi D/\Gamma_\Lambda) \tag{51}$$

Due to the above mentioned difference in tunnel matrix elements, $\Gamma^T > \Gamma^S$ the flow trajectories $E_S(D)$ and $E_T(D)$ may intersect. The necessary conditions for such level inversion in the situations illustrated by Fig. 6b,c are discussed in [26].

The physical reason for the level crossing is relatively transparent: tunnelling from DQD to metallic leads induces indirect electron exchange between two wells, and this "kinetic exchange" favors parallel aligning of spins in each well. If this "ferromagnetic" coupling overcomes antiferromagnetic indirect coupling $2\beta_i V$ in (25), (26), the S/T transition occurs due to accidental degeneracy, which stems from the dynamical $SO(4)$ symmetry of $\mathcal{H}_{dot}$.

Apparently, S/T transition is a widespread phenomenon in the physics of quantum dots with even occupation. It was observed in vertical dots [39], in lateral dots [37, 55, 56], in quantum rings [57] and discussed in many theoretical studies

[41, 58, 59, 60, 61, 62]. One should note that the enhancement of Kondo temperature in the crossover region mentioned above is accompanied by more refined manifestations of the pertinent accidental degeneracies.

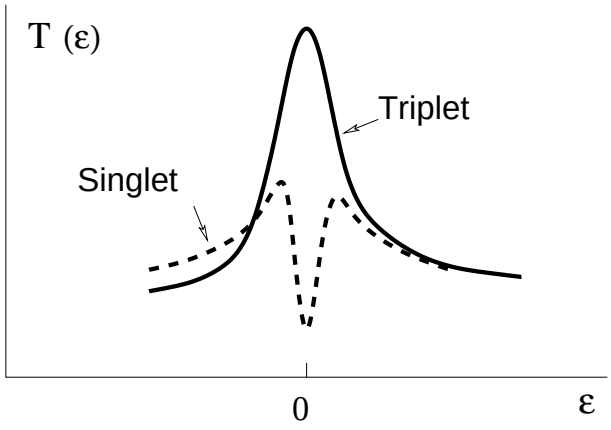

Figure 8: Tunnelling transparency of QD with even occupation on triplet (solid line) and singlet (dashed line) side of T/S crossover.

Indeed, on the triplet side of the Kondo cotunneling regime, one deals with *underscreened* $S = 1$ Kondo model [63], where only half of the impurity spin is dynamically screened by conduction electrons, provided the transformation (41) eliminates one of the two tunnel channels (otherwise the screening is complete). The role of low-lying singlet excitation is manifested by a modification of the Kondo temperature $T_K(\Delta_s)$ [see Eq. (49) and discussion around]. On the singlet side of this transition where $\Delta_s > 0$, formation of singlet ground state is a two-stage process [58]. Until the characteristic energy ε or temperature T exceeds $\Delta_s > 0$ the spin $S = 1$ is still underscreened, Kondo resonance in cotunneling enhances the transmission coefficient $\mathcal{T}(\varepsilon)$, so the latter grows with decreasing ε. This growth ceases at $\varepsilon \sim \Delta_s$, and $\mathcal{T}(\varepsilon)$ falls off rapidly, because at zero energy/temperature the Kondo regime is completely quenched. Thus, the ZBA of the conductance should have a form of a narrow Kondo peak like at the triplet side of the S/T transition, however, a pronounced dip should emerge at low energies $\varepsilon < \Delta_s$, so that conductance disappears at zero energy (see Fig.8). Such behavior was reported in [58] for a DQD in the parallel geometry (Fig. 6b) employing methods of numerical renormalization group (NRG) [64]. Later on, a similar behavior was substantiated for a planar QD with anomalously small interlevel spacing $\delta\varepsilon$ [62]. In this case, the intradot exchange J_d nearly compensates $\delta\varepsilon$ (see upper line in Eq. 37), the gap Δ_s is close to zero and the S/T transition may be induced by an external magnetic field applied perpendicular to the plane of the dot. One may neglect the Zeeman shift in comparison with orbital effects due to the small value of the g-factor in GaAs . Consequently, the ZBA peak in the conductance as a function of Δ_s should have a

pronounced maximum at $\Delta_s = 0$ with asymmetric slopes at the singlet and triplet sides of this crossover (Fig. 9). Apparently, all above effects were observed in the experiment [37].

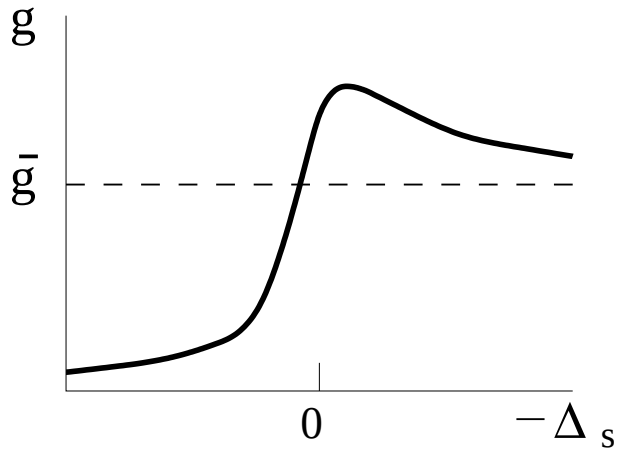

Figure 9: Conductance of QD with even occupation as a function of exchange gap Δ_s at fixed temperature T. $\bar{g}$ is a limiting value of conductance for completely quenched singlet, $|\Delta_s| \to \infty$.

A two-stage Kondo effect may occur also on the triplet side of the S/T transition in planar QD due to the difference between the tunnelling amplitudes for the levels ε_1 and ε_2 [60]. In this case, one has two tunneling channels for each lead characterized by the coupling constants $W_{1l}, W_{1r}, W_{2l}, W_{2r}$. The 2×2 tunnelling matrix can be diagonalized by a transformation similar to (41). Then one is left with two channels instead of four. These two channels are sufficient for a complete screening of the spin S=1. To describe the screening of a spin rotator under these conditions, one may use the mathematical option of representing the group $SO(4)$ as a direct product $SU(2) \times SU(2)$. This can be carried out by a simple transformation [2, 3, 26, 60]:

$$\mathbf{S} = \mathbf{s}_1 + \mathbf{s}_2, \quad \mathbf{R} = \mathbf{s}_1 - \mathbf{s}_2. \tag{52}$$

Here $\mathbf{s}_{1,2}$ are two fictitious spins 1/2 operators. Then the original problem can be mapped on the two-site Kondo problem, where each spin is coupled to the reservoir with its own exchange constant, $J_1 \neq J_2$. Unlike the case encountered in the conventional two-impurity Kondo effect [65], these fictitious spins are not independent, but the RG equations still may be derived, and the two-stage Kondo screening means that each channel is characterized by its own Kondo temperature $T_K(J_i)$. As a result, the unitarity limit is reached first in the channel with larger J_i, so that half of the spin 1 is screened, and then the remaining part of this spin is screened at lower temperatures. As a result, the conductance versus temperature curve acquires a stepwise form.

All these characteristics can be regarded as direct manifestations of dynamical $SO(4)$ symmetry inherent in the S/T multiplet. The picture becomes even richer when a parallel magnetic field is applied. a Zeeman splitting has a special role in the context of dynamical symmetry within the physics of Kondo cotunnelling through QD. These features are discussed in the next subsection.

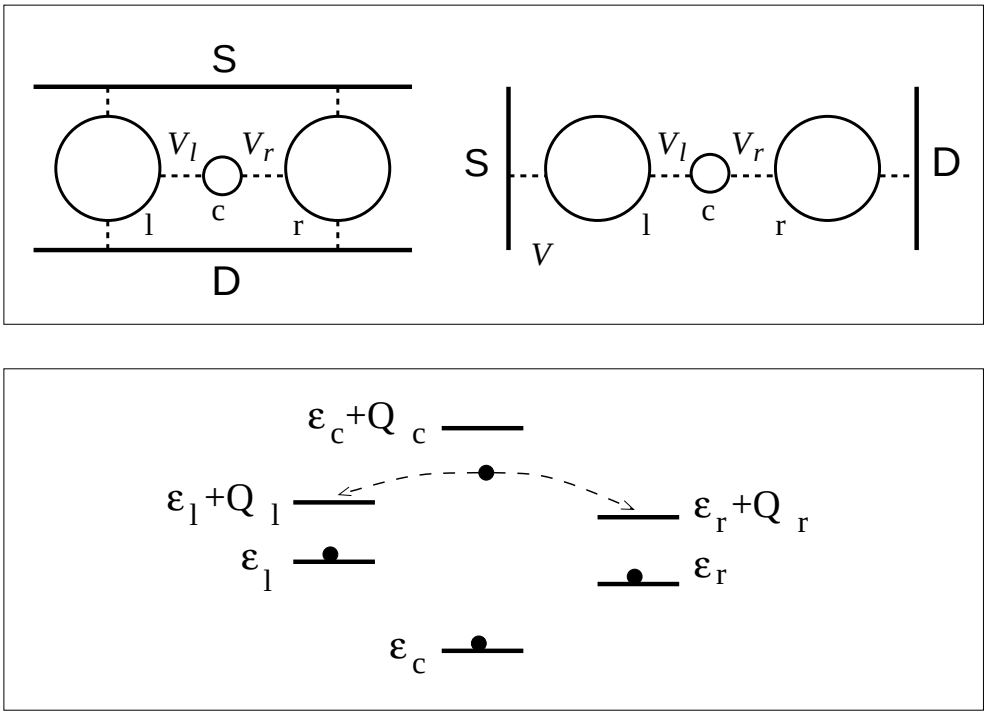

Figure 10: Top panel: TQD in parallel and series geometry. Lower panel: energy levels of isolated TQD occupied by four electrons. The last electron is poised between the left and right dot.

More refined cases of accidental degeneracy within spin multiplets arise in complex QD containing more than two valleys. One of such examples, a triple quantum dot (TQD) was considered in Ref. [33]. One can arrange a TQD both in parallel and in series geometry (see Fig. 10a,b). It possesses a richer low-energy spectrum than DQD and planar QD structures considered above. In particular, if the central dot has a smaller size (and hence larger value of Coulomb blockade parameter Q_c), than the side dots, and if the latter two are identical, then, beside other features, the isolated TQD has an additional mirror symmetry.

Let us discuss the representative case of TQD with even occupation $\mathcal{N}_0 = 4$ (see Fig. 10c for the energy level scheme). Then three electrons occupy the levels $\varepsilon_l, \varepsilon_c, \varepsilon_r$ and the last one is shared between the states $\varepsilon_i + Q_i$ $(i = l.r)$ avoiding the central well due to its high charging energy. When the inter-well tunnelling amplitudes $V_{l,r}$ are

taken into account, five low-energy states determine the dynamical symmetry: these are two singlets, two triplets and one charge transfer exciton. The mirror symmetry of such TQD may be broken by the gate voltages applied to the l and r wells. Then, the above mentioned Haldane-Anderson two-stage RG procedure applied to the system TQD + leads results in flow diagrams for these levels. Depending on the initial conditions, one encounters various cases of accidental degeneracy, which are connected with numerous $SO(n)$ groups. In the completely symmetric case, the relevant group is $P \times SO(4) \times SO(4)$ (two singlets and two triplets entering the effective SW Hamiltonian). Here P stands for the $l - r$ permutation operator describing the mirror symmetry of the TQD. Another interesting cases which arise when the mirror symmetry is broken are described by the familiar $SO(5)$ group (two singlets and one triplet) and by a more exotic $SO(7)$ group (two triplets and one singlet). The effective SW Hamiltonian for Kondo cotunneling is an obvious generalization of (36):

$$\mathcal{H}_{cot} = \sum_{\alpha\beta} \left(J^{(1)}_{\alpha\beta} \mathbf{S}_{\alpha\beta} \cdot \mathbf{s}_{\alpha\beta} + J^{(2)}_{\alpha\beta} \mathbf{R}_{\alpha\beta} \cdot \mathbf{s}_{\alpha\beta} \right). \tag{53}$$

$(\alpha, \beta = l, r)$. The number of vertices in this Hamiltonian is predetermined by the number of vectors in the Fock space for the $SO(n)$ group.

A general phase diagram of the TQD system is presented in Fig. 11. One may find in Ref. [33] the full list of group generators and various scaling equations with solutions for T_K specific for each dynamical group. As a result, in addition to the S/T transition, which in this phase diagram is a transition between the $SO(3)$ and the (shaded) singlet domains, one gets a rich variety of other transitions and continuous crossovers, which may be tested experimentally by changing gate voltages v_{gi} and tunnel rates Γ_i and observing the variation of the ZBA peak as a function of these parameters and temperature.

3.2 Kondo cotunnelling in an external magnetic field

In the previous section we discussed the role of magnetic field as a source of accidental level degeneracy due to diamagnetic shift (21) of single electron levels in QD. Here we discuss its role as a source of Zeeman splitting. Zeeman effect directly influences the symmetry properties of spin states because it violates rotational invariance. Its contribution to conventional Kondo effect is well known [45, 47, 66]. Due to lifted Kramers degeneracy of the impurity spin 1/2 state, the external magnetic field splits the Abrikosov-Suhl resonance into two peaks and eventually suppresses the Kondo effect, when the Zeeman splitting E_Z essentially exceeds $k_B T_K$. Dynamical symmetry inherent in QD may radically change this relatively simple picture. The most striking effect of magnetic field on quantum tunnelling through QD is a *magnetic field induced Kondo effect*, which is absolutely counterintuitive from the point of view of conventional Kondo physics. This effect predicted in [40] and immediately

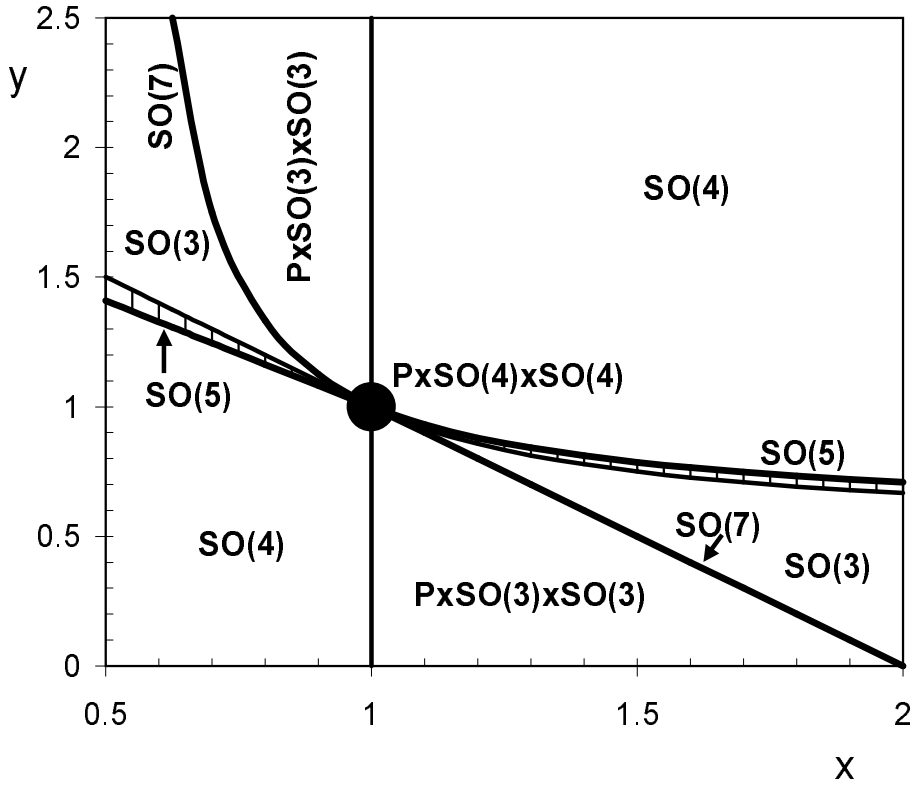

Figure 11: Dynamic symmetries in TQD: Phase diagram in coordinates $x = \Gamma_l/\Gamma_r$, $y{=}(\varepsilon_l{-}\varepsilon_c)/(\varepsilon_r{-}\varepsilon_c)$.

confirmed experimentally [38] on single-wall nanotubes was in fact the first explicit manifestation of dynamical symmetry in Kondo tunnelling.

The physical mechanism of magnetic field induced Kondo tunnelling in QD with even occupation is rather transparent. In the absence of strong exchange forces, the ground state of such QD is spin singlet (see above), and the lowest excited state is a triplet (see Figs. 3c and 6). These two states are separated by the spin excitation with the gap energy Δ_s (37). The Zeeman splitting energy E_Z may compensate this gap for the triplet state with spin up projection and thus result in an accidental degeneracy of a spin multiplet (Fig. 12). Mathematically, this means that the symmetry of a non-compact group $SO(4) = SU(2) \times SU(2)$ is reduced to an $SU(2)$ symmetry of the degenerate $\{S, T1\}$ "doublet". This reduction can be described in terms of generators of a dynamical group [26] by means of the vector operator $\mathbf{P}_1$ with components,

$$P_1^+ = \sqrt{2}X^{1S}, \quad P_1^z = X^{11} - X^{00}, \tag{54}$$

which generates the $SU(2)$ subgroup describing the doublet E_S, E_{T1}. The comple-

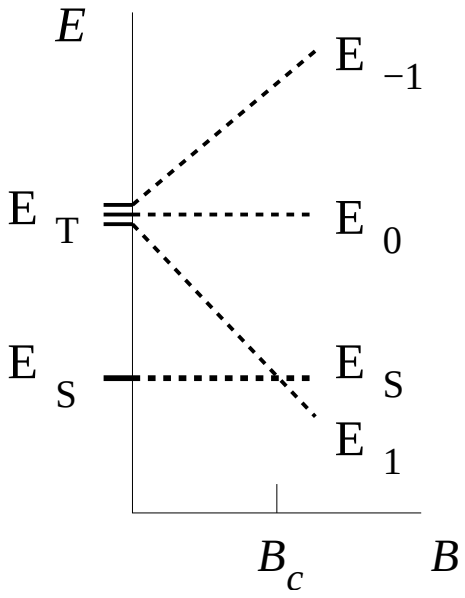

Figure 12: DQD: accidental degeneracy in Zeeman field.

mentary vector operator $\mathbf{P}_2$ defined as

$$P_2^+ = \sqrt{2}X^{0\bar{1}}, \quad P_2^z = X^{00} - X^{\bar{1}\bar{1}}, \tag{55}$$

generates a second subgroup $SU(2)$. Then the effective Hamiltonian describing Kondo cotunnelling induced by magnetic field in this QD has the form,

$$H^Z_{cotun} = E_G P_0 + J^{(2)} \mathbf{P}_1 \cdot \mathbf{s} \ . \tag{56}$$

This Hamiltonian should be compared with that of equation (36). Here $P_0 = X^{11} + X^{00}$ and $E_G = E_S = E_{T1}$ is the degenerate ground-state energy level of a QD in a "resonant" Zeeman field B_c. The Hamiltonian (56) describes Kondo-like tunnelling, which arises at $E_z = \Delta_s$ and disappears once the resonance conditions are not met. Precisely this effect was observed in measurements of conductance through a segment of nanotube confined by two metallic electrodes [38]. The Kondo-type ZBA in the Coulomb windows with even N was absent at zero B, then suddenly appeared at $B = B_c = 1.38$ T and afterward disappeared again at $B > B_c$.

A similar situation is possible in TQD [33]. However, in this more complicated structure, additional accidental approximate degeneracy between two singlet levels, e.g., E^l_S and E^r_S and one triplet state, e.g., E^r_{T1} is feasible. In this case the symmetry of TQD in magnetic field B_c is $SU(3)$ [see Eqs. (13), (14)], Kondo tunnelling violates this symmetry, and the corresponding cotunneling Hamiltonian is *generically anisotropic*. Similar situation arises when the Zeeman splitting induces crossing of two triplet states E^l_T and E^r_T with one singlet state, say E^r_S.

Another example of unusual sensitivity of conductance to Zeeman effect in lateral QD with even occupation was discussed in [62]. As was shown in Section II.A [see also discussion around Eq. (52)], the conductance in this case is predetermined by existence of two tunnelling channels, since two single electron levels $\varepsilon_{1,2}$ are involved in formation of S/T multiplet. Tunnelling through each of these levels is characterized by the scattering phase shift $\delta_{n\sigma}$ [35, 67], and the conductance can be expressed via these phase shifts at the Fermi energy ($n = 1, 2$). For example, in a specific case $W_{l1} = -W_{r1},\ W_{l2} = W_{r2}$ this expression is especially simple:

$$g(B) = \frac{1}{2}\sum_{\sigma} \sin^2(\delta_{2\sigma} - \delta_{1\sigma}). \tag{57}$$

Zeeman splitting results in repopulation of the levels $\varepsilon_{n\sigma}$. In a singlet state $\delta_{1\sigma} = \pi$, $\delta_{2\sigma} = 0$ for both spin projections σ. At finite B these shifts evolves under Friedel-Langer sum rule constraint

$$\sum_{n\sigma} \delta_{n\sigma}(B) = 2\pi,$$

in compliance with the occupation number $\mathcal{N} = 2$. As a result of this repopulation the conductance as a function of the magnetic field B acquires a highly non-monotonous dependence with a maximum occurring within the S/T crossover region.

To conclude this subsection, we emphasize that the main role of magnetic field is that it leads to violation of rotational symmetry in spin space. This violation results in the appearance of magnetic anisotropy of Kondo cotunnelling observables and non-trivial dynamical symmetries from $SU(n)$ family.

4 Dynamical symmetries at finite frequencies

Various manifestations of broken dynamical symmetry of quantum dots in the Kondo regime discussed in Section III were related to the low-energy sector of the spin excitation spectrum scaled by the Kondo temperature T_K. In principle, one may imagine a situation where the accidental degeneracy of energy levels arises in some limited interval separated by finite energy from the ground state of a nanoobject. Tunnelling into and out of electron reservoirs at finite energies should then be described by an effective Hamiltonians operating in the pertinent chosen interval $\Delta\varepsilon$. An appropriate method for studying dynamical properties of such systems is, for example, functional RG approach where a given Hamiltonian is diagonalized by continuous unitary transformation [68].

However, if one intends to remain within a definite manifold of discrete eigenstates of the QD, a frequency dependent perturbation should keep the system in quasiequilibrium, where the response is still determined by the thermodynamic partition function rather than by essentially non-equilibrium distribution functions of

the electrons in the leads. This restriction includes the experimentally important probe, that is, an interaction with a monochromatic electromagnetic field.

Now the question is, what kind of dynamical symmetry might prevail in photo-excited states, i.e., at finite excitation energy $h\nu$ of an absorbed light quantum. The main mechanism of light absorption in QDs is formation of excitons. Internal hidden symmetry of exciton spectra was briefly discussed in Subsection II.C in connection with multiexciton absorption in semiconductor nanoclusters. Here we focus our attention on dynamical effects involving Kondo processes and address the problem of *whether it is possible to observe Kondo effect at energies* $h\nu \gg T_k$.

The Kondo effect in the presence od an alternating electromagnetic field was intensively studied during the last decade [69]. In these studies, the interest was focused on the interaction between spin degrees of freedom of the QD on the one hand, and electron-hole photo-excitations in the leads on the other hand. The main effect of coherent light absorption in the leads is reflected through the occurrence of higher Kondo harmonics in the tunnel current as a response to the corresponding harmonics in the metallic band continuum (see recent review [70] for general view on the photon-assisted transport through QDs). Yet, from the point of view emphasized here, this interesting effect is not related directly to the dynamical symmetries of the QD. Indeed, the object of our interest has to do with the manifold of eigenstates of the QD, so we will discuss the Kondo aspects of excitonic states created by resonance light absorption *in the quantum dot itself*.

The problem of *dynamically induced Kondo effect* in QD with even occupation $\mathcal{N}$ was formulated in Ref. [71]. The theory was addressed first of all to systems composed of semiconductor nanoclusters (see Subsection II.C). The ground state of such nanocluster is fully occupied valence states divided by the energy gap Δ_g from the empty conduction states, so that the occupation N is always even. External visible light with $h\nu \sim \Delta_g$ may create electron-hole pairs (excitons) but the occupation of a QD remains, of course, even. The Hamiltonian responsible for creation of electron-hole pairs has the form

$$\mathcal{H}' = \sum_{cv} \sum_{\sigma} D_{cv} d^{\dagger}_{c\sigma} d_{v\sigma} \exp(-i\omega t) + h.c. \tag{58}$$

Here D_{cv} is the matrix element of the dipole operator $\hat{D}$, while the indices c, v stand for electrons in conduction and valence levels, respectively . This term should be added to the conventional Anderson Hamiltonian $\mathcal{H}_{dot} + \mathcal{H}_{tun}$. To demonstrate the mechanism of dynamically induced Kondo tunnelling, it is sufficient to retain in $\mathcal{H}_{dot}$ only the ground state $|0\rangle$ and the lowest singlet exciton

$$|E\rangle = \frac{1}{\sqrt{2}} \sum_{\sigma} d^{\dagger}_{c\sigma} d_{v\sigma} |0\rangle, \tag{59}$$

(triplet excitons remain dark in the context of optical transitions). One may then substitute the configuration changing operator X^{E0} for $d^{\dagger}_{c\sigma} d_{v\sigma}$ in the Hamiltonian

(58). The tunnel Hamiltonian intermixes the states $|0\rangle$ and $|E\rangle$ with the continuum states

$$|kc\rangle = \frac{1}{\sqrt{2}}\sum_{\sigma} d^{\dagger}_{c\sigma}c_{k\sigma}|0\rangle, \;\; |kv\rangle = \frac{1}{\sqrt{2}}\sum_{\sigma} c^{\dagger}_{k\sigma}d_{v\sigma}|0\rangle. \tag{60}$$

Using these definitions, $\mathcal{H}_{tun}$ can be written in terms of new configuration changing operators,

$$H_t = V_c\sum_k \left(|kc\rangle\langle 0| + \frac{1}{\sqrt{2}}|kv\rangle\langle E|\right) + V_v\sum_k \left(|kv\rangle\langle 0| - \frac{1}{\sqrt{2}}|kc\rangle\langle E|\right) + H.c. \tag{61}$$

The building blocks for the secular equation, which determine the response function $R(\epsilon)$

$$R(\epsilon) = \langle 0 \left| \hat{D}\frac{1}{\epsilon - \mathcal{H}}\hat{D}\right| 0\rangle, \tag{62}$$

are shown in Fig. 13. One immediately recognizes the two intermediate states as the first terms of a Kondo series for a state with one excess electron and one excess hole in the QD. To lowest order in $V_{c,v}$, this secular equation reads,

$$\det\left|\begin{array}{cc} \epsilon - \Sigma_{00}(\epsilon) & -\Sigma_{E0}(\epsilon) \\ -\Sigma_{0E}(\epsilon) & \epsilon - \Delta - \Sigma_{EE}(\epsilon)\end{array}\right| = 0. \tag{63}$$

The real parts of the self energies contain the familiar Kondo logarithmic divergencies

$$\mathrm{Re}\Sigma_{jl}(\epsilon) \sim \frac{\Gamma_{jl}}{2\pi}\ln\frac{(\epsilon - \Delta_{c,v})^2 + (\pi T)^2}{D^2},$$

with $\Gamma_{jl} = \pi\rho_0 V_j^* V_l$. These functions have sharp maxima at energies $\Delta_{c,v} = \Delta_g - \varepsilon_{c,v}$, which can be considered as "precursors" of Kondo peaks in a weak coupling regime $T \gg T_K$.

The secular equation (63) describes a dynamical mixing between the states $|0\rangle$ and $|E\rangle$ with maxima at finite frequencies $h\nu \sim \Delta_{c,v} \gg T_K$ within the multiplet of eigenstates of the QD. This scenario has no analogs in our previous examples of broken dynamical symmetry. Here, the Kondo processes arise only in the intermediate states of light absorption, when either 1 or 3 electrons occupy the relevant levels of the QD (Fig. 13), whereas there is no Kondo screening in the initial and final states of exciton absorption due to the even occupation $\mathcal{N}_i$ and $\mathcal{N}_f$. The above maxima of the self energies should be observed as satellite peaks in optical lineshape $\sim$ Im $R(h\nu)$ at energies $\Delta_{c,v}$, which accompany the main peak of exciton absorption at $h\nu \sim \Delta_g$. In spectroscopic nomenclature these midgap excitonic states may be regarded as "Kondo shake-up peaks".

An important constraint is imposed on dynamical Kondo screening by the finite lifetime of electrons and holes in the photoexcited QD. Indeed, too short photoelectron, photo-hole or photo-exciton lifetimes, $\tau_l < \hbar(k_B T_K)^{-1}$, prevents even the formation of a precursor of the Kondo resonance, not to mention the impossibility of

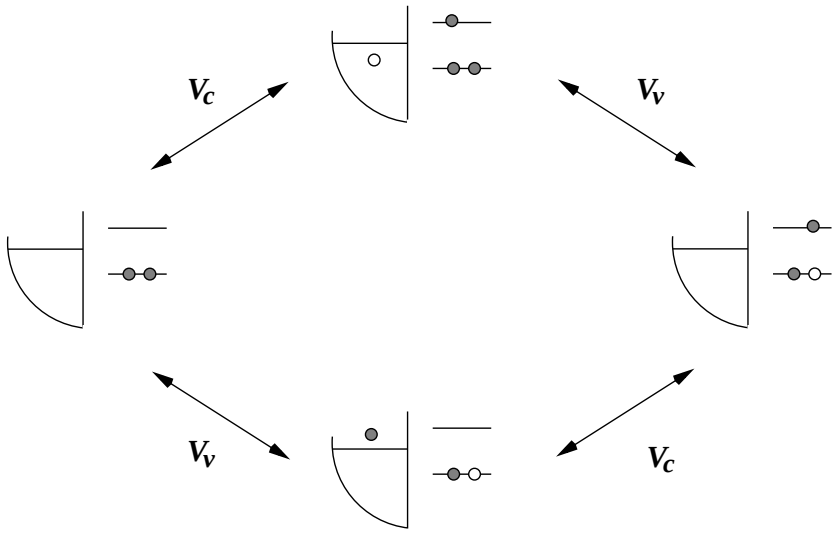

Figure 13: Building blocks of secular equation (62).

reaching the strong coupling Kondo regime. To ensure conditions for the observation of shake-up Kondo satellites, one should design the heterostructure lead/dot/lead in such a way that at least one of the two carriers in the QD has a negligible tunnelling width (we refer the reader to Ref. [71] for a detailed analysis of this problem). The problem of finite lifetime for excited Kondo states will be addressed in more details in the next section.

In principle, dynamically induced Kondo effect may arise not only in excitonic spectra, but also in photoemission spectra, where the electron leaves the QD for the metallic lead under light irradiation [72]. In this case only two blocks from Fig. 13 are involved in dynamical mixing, namely the ground state $|0\rangle$ and the state with excess hole $|kv\rangle$ in a QD. This mixing manifests itself as an edge singularity in the absorption spectrum

$$\text{Im } R(h\nu) \sim (h\nu - \Delta_{cv})^{\alpha}$$

where the power α is predetermined by the phase shift of electrons on the Fermi level of the lead. In case of inverse process, when the excess electron is captured by the dot with light quantum emission, the state $|kc\rangle$ is involved in dynamical mixing. Of course, all these shake-up processes go back to the celebrated edge-singularity in

X-ray absorption spectra discovered theoretically in mid sixties [73].

The dynamical mixing processes discussed above arise in linear response to external electromagnetic field. It is clear that similar processes may arise also in non-linear optical response, but the variety of possibilities is richer in this case. One such possibility, which may be realized in pump-probe spectroscopy was discussed in Ref. [74]. According to the proposal outlined therein, a strong monochromatic pumping field with frequency ν_1 modifies the position of the deep electron level in the dot, $\varepsilon_d \to \varepsilon_d + h\nu_1$, and induces a Kondo-resonance on the Fermi level described by the self-consistent equation

$$\epsilon = \Sigma(\epsilon)$$

(cf. Eq. (63). The quantity $\pi\rho_0(\bar{d}\mathcal{E}_1)^2$ can be interpreted as "tunnelling width" Γ in the self energy $\Sigma(\epsilon)$ ($\bar{d}$ is the dipole moment and $\mathcal{E}_1$ is the amplitude of the probe electric field). On top of it one should measure the probe light absorption. The analysis of third order pump-probe polarization shows that when the resonance condition $\nu_1 \simeq \nu_2$ is valid, a dynamical mixing between the pumped level $E_d = \varepsilon_d + h\nu_1$ and the Kondo resonance at the absorption threshold $h\nu_2 = \varepsilon_F - \varepsilon_d$ arises. As a result, a narrow shake-up satellite appears below the absorption threshold.

One more peculiar possibility of Kondo shake-up processes for *charged* excitons was discussed in Ref. [75]. Charged exciton is a multiparticle complexes consisting of several valence holes and conduction electrons trapped in a self-consistent potential well. Such excitons containing one hole and $n+1$ electrons are observed in self-assembled InAs/GaAs quantum dots discussed in Section II.C [76]. These complexes are usually labelled as X^{n-}. The surface of wetting GaAs layer may be filled with 2D electrons, and tunnelling between the trap and the 2D electron continuum is possible. Some of these excitons have non-zero spin, so the possibility of Kondo screening opens up. According to Ref. [75], the best candidate for Kondo screening is the X^{2-} exciton, which possesses nonzero spin and sufficiently long lifetime necessary to form a screening Kondo cloud. This exciton consists of a hole in an s state and three electrons (two of them are in s-states and one in a p-state). Electron tunnelling between the trap and the 2D electrons in the wetting layer admixes the state $|X^{3-}c_{ks}|0\rangle$ with an additional electron captured into the trap to the state $|X^{2-}|0\rangle$ in analogy with Eqs. (60),(61). The narrow shake-up peak arises in the photoluminescence spectrum as a result of Kondo screening like in the cases discussed above. Hybridization between these states induced by photon emission was registered experimentally in photoluminescence spectrum measured in a strong magnetic field, where the 2D electronic states become discrete due to Landau quantization, and the excitonic levels are subject to diamagnetic shift [77]. Of course, there is no room for Kondo effect in case of fully discrete spectrum, but the dynamical hybridization seems to become an established fact.

5 Dynamical symmetries in non-equilibrium state

Unlike the problem of magnetic scattering in doped metals, where the Kondo effect in a strong coupling regime is described in terms of equilibrium thermodynamics both in the strong coupling ($T \ll T_K$) and in the weak coupling ($T > T_K$) limits, Kondo tunnelling through QD may occur also under non-equilibrium conditions [78]. We discussed in Section IV the special case of Kondo effect under the influence of a monochromatic ac field, which is applied either on the leads or to the QD. Here we turn our attention to the case, where equilibrium conditions are violated by the finite bias applied on the metallic leads.

There is an extensive literature on the Kondo tunnelling through QD under non-equilibrium conditions. Referring the reader to recent papers [79], where this problem is discussed in details, we concentrate here only on the manifestations of dynamical symmetry violation in non-equilibrium Kondo effect. Such a possibility arises when the S/T transitions *induced by finite bias* are involved in Kondo cotunneling [80].

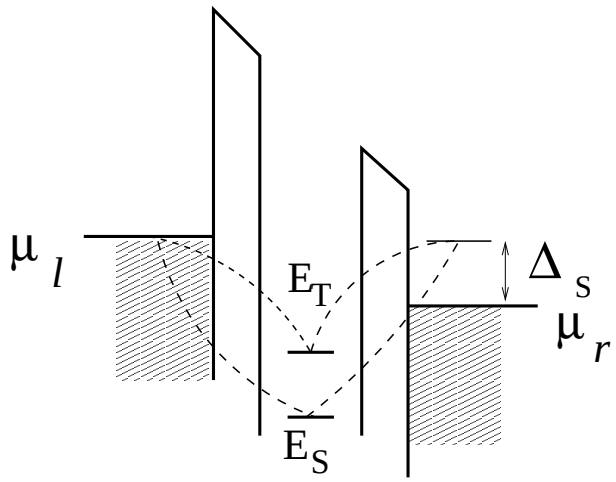

Figure 14: DQD at finite bias.

To be concrete let us consider a T-shaped double quantum dot (Fig. 5c) as an example of an experimental setup, where an *electric field induced Kondo effect* can be realized. The S/T energy gap Δ_s in a T-shaped DQD (37) is controlled by the height and width of the barrier separating the two dots. The tunnelling amplitude W between the DQD and the metallic contacts is controlled by gate voltages generating the corresponding barriers. If the total number of electrons $\mathcal{N} = 2n$ is even and $\Delta_s \gg T_K^{eq}$, where T_K^{eq} characterizes the equilibrium Kondo temperature of an underscreened $S = 1$ Kondo effect, the ground state of the dot is a singlet and there is no Kondo enhancements of the differential conductance associated with co-tunnelling processes in equilibrium (infinitesimally small voltage between source

and drain). However, a finite bias applied to the leads changes this situation dramatically. The electrons, accelerated by the bias v_b, gain an additional energy $\sim ev_b$ which may compensate the energy Δ_s necessary for spin flips, and thus make Kondo co-tunnelling possible (see Fig. 14 where the processes involved in cotunneling are shown by dashed lines). Recalling that the pertinent charge conserving system is not the isolated dot, but, rather, the closed circuit composed of source-dot-drain, we may draw the conclusion that the non-equilibrium Kondo tunnelling, which develops in a "moving frame" of a system with dynamical symmetry results in a finite bias anomaly (FBA) in contrast with the ubiquitous ZBA characteristic for the conventional (equilibrium) Kondo effect.

To characterize non-equilibrium Kondo effect in DQD, we adopt the $SO(4)$ Kondo Hamiltonian (53). This Hamiltonian can be derived for nonzero bias with the help of out of equilibrium SW transformation ([52]). As a result, at small bias (linear response regime) the exchange integrals $J^{\Lambda\Lambda'}_{\alpha\alpha'}$ become time-dependent, but the scaling equations can be derived from the condition of the invariance of the linear conductance. However, the Hamiltonian (53) may be derived in a different fashion assuming that both leads remain in quasi equilibrium and possess their own chemical potentials $\mu_{L,R}$ under the constraint $\mu_L = \mu_R + eV$. The relaxation processes in the leads are negligible provided the leads are sufficiently hot and phonon-assistant thermalization processes are fast enough compared with other characteristic time scales involved in this analysis. This fact allows us to adopt an RG procedure for frequency - dependent vertices ([79]). However, the dynamical symmetry of the problem implies a possible further simplification of the RG scheme. The key distinction between the formalism suggested in Ref. ([80]) for DQD and the Keldysh type description of an $s = 1/2$ dot in an external magnetic field under non-equilibrium condition [79, 81] is this: In the first case, the presence of an additional adjustable parameter, namely $|\Delta_s - eV|$ justifies the *standard* RG scheme if the resonance condition $|\Delta_s - eV| \ll T \ll T_K^{eq}$ is fulfilled. Therefore, under non-equilibrium conditions illustrated by Fig. 14, the dynamical symmetry backs the quasi-equilibrium RG approach generally inapplicable to conventional Kondo effect out of equilibrium.

As a result, the equations for tunnelling vertices $J^{\Lambda\Lambda'}_{\alpha\alpha'}$ at finite temperatures are written as follows:

$$\frac{d\mathcal{J}^T_{ll}}{dL} = -\rho_0(\mathcal{J}^T_{ll})^2, \quad \frac{d\mathcal{J}^{ST}_{ll}}{dL} = -\rho_0\mathcal{J}^{ST}_{ll}\,\mathcal{J}^T_{ll}, \tag{64}$$

$$\frac{d\mathcal{J}^T_{lr}}{dL} = -\rho_0\mathcal{J}^T_{ll}\,\mathcal{J}^T_{lr}, \quad \frac{d\mathcal{J}^{ST}_{lr}}{dL} = -\rho_0\mathcal{J}^{ST}_{ll}\,\mathcal{J}^T_{lr},$$

$$\frac{d\mathcal{J}^S_{lr}}{dL} = \frac{1}{2}\rho_0\left(\mathcal{J}^{ST}_{ll,+}\mathcal{J}^{TS}_{lr,-} + \frac{1}{2}\mathcal{J}^{ST}_{ll,z}\,\mathcal{J}^{TS}_{lr,z}\right) \tag{65}$$

(cf. Eq. 47). The solution of the system of equations (65) supplemented by the

boundary condition $\mathcal{J}^{\Lambda\Lambda'}_{\alpha\alpha'}(D_0) = J^{\Lambda\Lambda'}$ are given by

$$\mathcal{J}^{T}_{\alpha,\alpha'} = \frac{J^T}{1-\rho_0 J^T \ln(D/T)}, \quad \mathcal{J}^{ST}_{\alpha,\alpha'} = \frac{J^{ST}}{1-\rho_0 J^T \ln(D/T)},$$

$$\mathcal{J}^{S}_{lr} = J^S - \frac{3}{4}\rho_0 (J^{ST})^2 \frac{\ln(D/T)}{1-\rho_0 J^T \ln(D/T)}. \tag{66}$$

and determine a new non-equilibrium Kondo temperature $T_K^{neq} \sim D\exp(-1/\rho_0 J^T)$ $\sim (T_K^{eq})^2/D$. This temperature should be compared with the relaxation rate τ_{ST}^{-1} determined by singlet-triplet transitions in the dot. The condition $\hbar/\tau_{ST} \ll T_K^{neq}$ defines a stability domain for the finite bias anomaly against the decoherence processes associated with effects of re-population of the dot by the finite bias. For realistic dots, the estimate $\hbar/\tau_{ST} \sim (\Delta_s)^3/D^2$ holds (see [80]), and the Kondo effect is robust in a broad domain of external parameters. This means that FBA arises at $eV \approx \Delta_s$ instead of conventional Kondo ZBA (see Fig. 15).

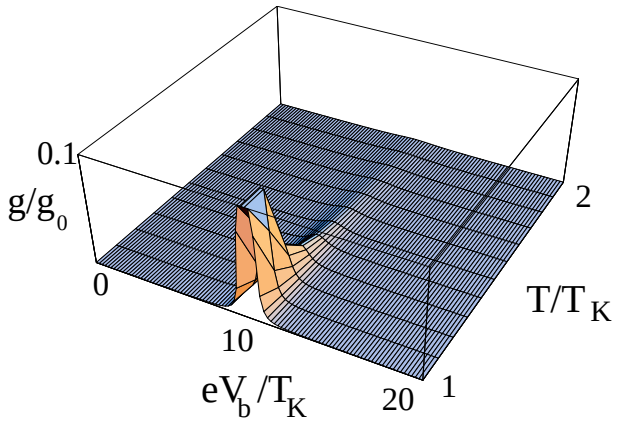

Figure 15: Finite bias anomaly (FBA) in double quantum dot. Here $g_0 = e^2/\pi\hbar$ is the unitarity limit for quantum conductance, which may be achieved at $T = 0$ under condition of perfect Kondo screening.

The perturbative corrections corresponding to re-population effects result in asymmetry of the FBA in the differential conductance. The origin of this asymmetry (threshold character of the relaxation associated with transitions between different components of the triplet state) is however different from that for the conventional non-equilibrium Kondo effect [79] and is also attributed to the hidden dynamical symmetries associated with the $SO(4)$ Kondo problem. The FBA of the type shown in Fig. 15 was observed in tunnel conductance of carbon nanotubes [82]

An interesting question which arises here is whether the non-equilibrium Kondo effect falls into the class of strong-coupling regime. It has been extensively studied during the last few years (see discussion and references in [79, 81]). The same question when addressed to systems characterized by hidden dynamical symmetries

allows a simple and straightforward answer: the strong coupling limit is not achievable in this situation. There is always an energy scale determined by an external bias, decoherence effects associated with AC or effects related to repopulation of the dot which prevent the system from both one-stage and two-stage Kondo scenario [58, 62] and suppress the Kondo effect in the ground state.

6 Addendum. Dynamical algebras

This chapter is a mathematical supplement to Chapter I. Here we clarify the origin of spin dynamical symmetries and describe several useful bosonization and fermionization procedures for the generators of $SO(n)$ groups.

To demonstrate specific properties of dynamical algebras and various representations of groups possessing hidden dynamical symmetries we consider a group of 4-dimensional rotations. We start with referring to the well known description of a hidden symmetry implicit in *spherical quantum mechanical rotator*. The Hamiltonian of rotator is

$$\mathcal{H}_r = \frac{1}{2I}\mathbf{L}^2 \tag{67}$$

where $\mathbf{L}$ is the operator of orbital moment and I is the moment of inertia.

Lie algebras $o(n)$ are defined on a basis of $\frac{1}{2}n(n-1)$ operators of infinitesimal rotation

$$D_{\alpha\beta} = -D_{\beta\alpha} = x_\beta \frac{\partial}{\partial x_\alpha} - x_\alpha \frac{\partial}{\partial x_\beta}, \qquad (\alpha < \beta = 1, 2, ...n) \tag{68}$$

which possess the following commutation relations

$$[D_{\alpha\beta} D_{\mu\nu}] = (\delta_{\alpha\mu} D_{\beta\nu} - \delta_{\alpha\nu} D_{\beta\mu} - \delta_{\beta\mu} D_{\alpha\nu} + \delta_{\beta\nu} D_{\alpha\mu}). \tag{69}$$

(see, e.g., [3, 83]. The antisymmetric tensor $D_{\alpha\beta}$ for $o(4)$ algebra acts in 4-dimensional space. It can be parametrized in terms of two vectors $\mathbf{L}$ and $\mathbf{M}$ as follows

$$-i \begin{pmatrix} 0 & L_3 & -L_2 & M_1 \\ & 0 & L_1 & M_2 \\ & & 0 & M_3 \\ & & & 0 \end{pmatrix} \tag{70}$$

where the infinitesimal operators of $SO(4)$ group [83] in 4-dimensional space (x, y, z, t) are given by

$$\begin{aligned} L_1 &= i\left(y\frac{\partial}{\partial z} - z\frac{\partial}{\partial y}\right), \quad L_2 = i\left(z\frac{\partial}{\partial x} - x\frac{\partial}{\partial z}\right), \quad L_3 = i\left(x\frac{\partial}{\partial y} - y\frac{\partial}{\partial x}\right), \\ M_1 &= i\left(t\frac{\partial}{\partial x} - x\frac{\partial}{\partial t}\right), \quad M_2 = i\left(t\frac{\partial}{\partial y} - y\frac{\partial}{\partial t}\right), \quad M_3 = i\left(t\frac{\partial}{\partial z} - z\frac{\partial}{\partial t}\right). \end{aligned} \tag{71}$$

¿From here we deduce the commutation relations:

$$[L_j, L_k] = ie_{jkl}L_l, \qquad [M_j, M_k] = ie_{jkl}L_l, \qquad [M_j, L_k] = ie_{jkl}M_l. \tag{72}$$

Six generators of $SO(4)$ group are defined in a 4-dimensional spherical coordinate system characterized by 3 angles θ, ϕ, α,

$$\begin{aligned} x_1 &= x = R\sin\alpha\sin\theta\cos\phi \quad x_2 = y = R\sin\alpha\sin\theta\sin\phi \\ x_3 &= z = R\sin\alpha\cos\theta \qquad\quad x_4 = t = R\cos\alpha. \end{aligned} \tag{73}$$

Returning back to spherical rotator, one may treat angle α as an angle between the rotation axis and fixed Cartesian z-axis. Two rest angles characterize rotation in a 3D subspace with fixed rotation axis. The operators of infinitesimal rotations are is given by

$$L_3 = -i\frac{\partial}{\partial\phi}, \qquad L^{\pm} = e^{\pm i\phi}\left(\pm\frac{\partial}{\partial\theta} + i\cot\theta\frac{\partial}{\partial\phi}\right),$$

$$M_3 = i\cos\theta\frac{\partial}{\partial\alpha} - i\sin\theta\cot\alpha\frac{\partial}{\partial\theta},$$

$$M^{\pm} = e^{\pm i\phi}\left(\cot\alpha\left[\mp\frac{1}{\sin\theta}\frac{\partial}{\partial\phi} + i\cos\theta\frac{\partial}{\partial\theta}\right] + i\sin\theta\frac{\partial}{\partial\alpha}\right),$$

where ladder operators $L^{\pm} = L_1 \pm iL_2$ and $M^{\pm} = M_1 \pm iM_2$. The angular moment $\mathbf{L}$ is parameterized by only two angles, θ, ϕ according to standard representation of $SO(3)$ group [84]. Although the Hamiltonian (67) contains only the invariant $\mathbf{L}^2$, describing 3D rotation, the hidden 4th dimension is accessible due to additional generator $\mathbf{M}$, which determines the transitions from 3D space to the true 4D manifold [85]. As a result the operator $\mathbf{L^2}$ is no more conserving quantity for $SO(4)$ group. The Casimir operator

$$\mathbf{L^2} + \mathbf{M^2} = -\frac{\partial^{\mathbf{2}}}{\partial\alpha^{\mathbf{2}}} - \mathbf{2}\cot\alpha\frac{\partial}{\partial\alpha} - \mathrm{cosec}^{\mathbf{2}}\alpha\left(\frac{\partial^{\mathbf{2}}}{\partial\theta^{\mathbf{2}}} + \cot\theta\frac{\partial}{\partial\theta} + \mathrm{cosec}^{\mathbf{2}}\theta\frac{\partial^{\mathbf{2}}}{\partial\phi^{\mathbf{2}}}\right) = \mathbf{3} \tag{74}$$

and the orthogonality condition

$$\mathbf{L}\cdot\mathbf{M} = \mathbf{M}\cdot\mathbf{L} = \mathbf{0} \tag{75}$$

determine the hyperspherical harmonics as the eigen functions of the angular part of 4-D Laplacian,

$$Y_{nlm}(\alpha,\theta,\phi) = i^{n-1-l}2^{l+1}l!\left[\frac{n(n-l-1)!}{2\pi(n+l)!}\right]^{1/2}\sin^l\alpha C_{n-l-1}^{l+1}(\cos\alpha)Y_l^m(\theta,\phi).$$

Here C_{n-l-1}^{l+1} is Gegenbauer polynomial [86] and $Y_l^m(\theta,\phi)$ stands for standard three dimensional spherical harmonics.

It is known, that three generators of $SU(2)$ group together with the Casimir operator $\mathbf{L^2}$ define a sphere S_2 where each state is parameterized by two angles. The coherent states of $SU(2)$ group may be constructed [87] by making a standard stereographical projection of the sphere from its south pole to the complex plane z. The space of generators of $SO(4)$ group is 6-dimensional, while 2 constraints determine 4-dimensional surface, where each state is characterized by four angles. The stereographical projection of this surface on a 4-D complex hyperplane allows to construct coherent states for $SO(4)$ group.

The commutation relations (72) can be transformed into another form by making the linear transformation to the basis

$$J_i = \frac{L_i + M_i}{2}, \quad K_i = \frac{L_i - M_i}{2} \tag{76}$$

giving more simple commutation relations

$$[J_j, J_k] = ie_{jkl}J_l, \qquad [K_j, K_k] = ie_{jkl}K_l, \qquad [K_j, J_k] = 0. \tag{77}$$

The operators L_i, M_i as well as J_i, K_i form the elements of the Lie algebra $o(4)$. The operators (J_1, J_2, J_3) and (K_1, K_2, K_3) are separately closed under commutations, each describing a subalgebra of $o(4)$, namely $o(3) = u(2)$. The Lie algebra $o(4)$ is the direct sum of two $o(3)$ algebras. This splitting of the $o(4)$ algebra into two $o(3)$ subalgebras is directly associated with the local isomorphism between the Lie group $SO(4)$ with the direct product group $SU(2) \times SU(2)$. The triads (J_1, J_2, J_3) and (K_1, K_2, K_3) each form proper ideals [83] in $o(4)$, and the Lie algebra $o(4)$ is semi-simple.

The symmetry group of *spin rotator* is defined in close analogy with the above construction, but all rotations are performed in a spin space. The triplet/singlet pair is formed in a simplest case by two electrons represented by their spins $s = 1/2$. Let us denote them as $\vec{s}_1$ and $\vec{s}_2$. The components of these vectors obey the commutation relations

$$[s_{1j}, s_{1k}] = ie_{jkl}s_{1l}, \qquad [s_{2j}, s_{2k}] = ie_{jkl}s_{2l}, \qquad [s_{1j}, s_{2k}] = 0 \tag{78}$$

In similarity with (77) these vectors may be qualified as generators of $o(4)$ algebra, which represents a spin rotator. Then, the linear combinations

$$S_i = s_{1i} + s_{2i}, \quad R_i = s_{1i} - s_{2i} \tag{79}$$

are introduced in analogy with (76), which define 6 generators of SO(4) group possessing the commutation relations (8). These generators are represented in terms of the Pauli-like matrices as follows

$$S^+ = \sqrt{2}\begin{pmatrix} 0 & 1 & 0 & 0 \\ 0 & 0 & 1 & 0 \\ 0 & 0 & 0 & 0 \\ 0 & 0 & 0 & 0 \end{pmatrix}, \quad S^- = \sqrt{2}\begin{pmatrix} 0 & 0 & 0 & 0 \\ 1 & 0 & 0 & 0 \\ 0 & 1 & 0 & 0 \\ 0 & 0 & 0 & 0 \end{pmatrix},$$

$$S^z = \begin{pmatrix} 1 & 0 & 0 & 0 \\ 0 & 0 & 0 & 0 \\ 0 & 0 & -1 & 0 \\ 0 & 0 & 0 & 0 \end{pmatrix}, \quad R^z = -\begin{pmatrix} 0 & 0 & 0 & 0 \\ 0 & 0 & 0 & 1 \\ 0 & 0 & 0 & 0 \\ 0 & 1 & 0 & 0 \end{pmatrix}, \tag{80}$$

$$R^+ = \sqrt{2}\begin{pmatrix} 0 & 0 & 0 & 1 \\ 0 & 0 & 0 & 0 \\ 0 & 0 & 0 & 0 \\ 0 & 0 & -1 & 0 \end{pmatrix}, \quad R^- = \sqrt{2}\begin{pmatrix} 0 & 0 & 0 & 0 \\ 0 & 0 & 0 & 0 \\ 0 & 0 & 0 & -1 \\ 1 & 0 & 0 & 0 \end{pmatrix}. \tag{81}$$

where the ladder operators $S^{\pm} = S^x \pm iS^y$, $R^{\pm} = R^x \pm iR^y$. The constraints (74), (75) now acquire the form

$$\mathbf{S}\cdot\mathbf{R} = 0, \qquad \mathbf{S}^2 + \mathbf{R}^2 = 3.$$

By construction $\mathbf{S}$ is the operator of the total spin of pair, which can take values $S = 0$ for singlet and $S = 1$ for triplet states. The second operator $\mathbf{R}$ is responsible for transition between singlet and triplet states. Thus we come to the dynamical group $SO(4)$ for spin rotator introduced in Chapter I [see Eqs. (7) and (8)].

Similar procedure is used for the $SO(5)$ group. The corresponding $o(5)$ algebra has 10 generators $D_{\alpha\beta} = -D_{\beta\alpha}$ (68) satisfying commutation relations (69). These 10 generators may be identified as 3 vectors and a scalar in a following fashion

$$-i\begin{pmatrix} 0 & S^z & -S^y & R^x & P^x \\ & 0 & S^x & R^y & P^y \\ & & 0 & R^z & P^z \\ & & & 0 & A \\ & & & & 0 \end{pmatrix} \tag{82}$$

where the operators $\mathbf{S}, \mathbf{R}, \mathbf{P}$ and the scalar operator A obey the following commutation relations

$$\begin{aligned} [S_j, S_k] &= ie_{jkl}S_l, \quad [R_j, R_k] = ie_{jkl}S_l, \quad [P_j, P_k] = ie_{jkl}S_l, \\ [R_j, S_k] &= ie_{jkl}R_l, \quad [P_j, S_k] = ie_{jkl}P_l, \quad [R_j, P_k] = i\delta_{jk}T, \\ [P_j, A] &= iR_l, \quad [A, R_j] = iP_j, \quad [A, S_j] = 0. \end{aligned} \tag{83}$$

[cf. Eqs. (8), (11)]. The operators $\mathbf{R}$ and $\mathbf{P}$ are orthogonal to $\mathbf{S}$, while the Casimir operator is $\mathcal{K} = \mathbf{S}^2 + \mathbf{R}^2 + \mathbf{P}^2 + A^2 = 4$. These operators act in 10-D spin space, and the kinematical restrictions reduce this dimension to 7. Similarly to $SO(4)$ group, the vector operators describe spin S=1 and transitions between spin triplet and two singlet components of the multiplet, whereas the scalar A stands for transitions between two singlet states. Then the vectors $\mathbf{R}$ and $\mathbf{P}$ may be identified with $\mathbf{R_1}$ and $\mathbf{R_2}$, and the spin algebra is connected with the algebra for Hubbard operators by equations (10).

The group $SO(5)$ is non-compact, and the parametrization (82) is not unique. As an alternative, one may refer to another representation of $D_{\alpha\beta}$ used, the theory of high-T_c superconductivity [92]:

$$-i\begin{pmatrix} 0 & & & & \\ \pi_x+\pi_x^\dagger & 0 & & & \\ \pi_y+\pi_y^\dagger & -S^z & 0 & & \\ \pi_z+\pi_z^\dagger & S^y & -S^x & 0 & \\ Q & -i(\pi_x^\dagger-\pi_x) & -i(\pi_y^\dagger-\pi_y) & -i(\pi_z^\dagger-\pi_z) & 0 \end{pmatrix} \tag{84}$$

with 10 generators identified as a scalar Q and three vectors $\vec{S}, \vec{\pi}$ and $\vec{\pi}^\dagger$ standing for the total charge, spin and π triplet $S=1$ superconductor order parameter. Both representations (82) and (84) are connected by the unitary transformation.

It is well known that the spin space may be projected onto bosonic or fermionic space by various transformations useful for specific physical applications. Here we show the way of generalization of several popular spin-boson and spin-fermion representations to the dynamical algebras $o(4)$ and $o(5)$. Like in the case of pure spin operators, these representations should preserve all kinematical constraints.

Schwinger [88] has shown that it is possible to make a realization of $SU(2)$ group for spin S in terms of boson operators $a_i, a_i^\dagger$, $(i=1...2S+1)$ with

$$[a_i, a_j^\dagger] = \delta_{ij}.$$

In particular, for $S=1/2$ Schwinger's bosonization reads

$$\vec{s} = \frac{1}{2} a^\dagger \vec{\tau} a, \qquad a^\dagger = (a_1, a_2). \tag{85}$$

($\vec{\tau}$ is the set of 2×2 Pauli matrices). One should introduce the local constraint $a_1^\dagger a_1 + a_2^\dagger a_2 = 1$ to get rid of spurious states associated with this bosonic representation.

Using local isomorphism of $SO(4)$ and $SU(2)\times SU(2)$, one may derive a representation of $SO(4)$ generators in terms of 4-component Schwinger bosons as

$$\vec{S} = \vec{s}_1 + \vec{s}_2 = \frac{1}{2}(a^\dagger \vec{\tau}_a a + b^\dagger \vec{\tau}_b b), \qquad \vec{R} = \vec{s}_1 - \vec{s}_2 = \frac{1}{2}(a^\dagger \vec{\tau}_a a - b^\dagger \vec{\tau}_b b) \tag{86}$$

where 4×4 τ-matrices act on $a-$ and $b-$ subsets of 4-vector $\mathbf{q}^T = (a_1^\dagger, a_2^\dagger, b_1^\dagger, b_2^\dagger)$.

An alternative approach is based on use of Abrikosov [46] or Popov-Fedotov [89, 90] auxiliary fermions f_λ, where $\lambda = -1, 0, 1, s$. Making use of (7) we represent 6 generators of $SO(4)$ as follows

$$\begin{aligned} S^+ &= \sqrt{2}(f_0^\dagger f_{-1} + f_1^\dagger f_0), \quad S^- = \sqrt{2}(f_{-1}^\dagger f_0 + f_0^\dagger f_1), \quad S^z = f_1^\dagger f_1 - f_{-1}^\dagger f_{-1}, \\ R^+ &= \sqrt{2}(f_1^\dagger f_s - f_s^\dagger f_{-1}), \quad R^- = \sqrt{2}(f_s^\dagger f_1 - f_{-1}^\dagger f_s), \quad R^z = -(f_0^\dagger f_s + f_s^\dagger f_0). \end{aligned}$$

with the only constraint

$$n_1 + n_0 + n_{-1} + n_s = 1 \ , \tag{87}$$

whereas the orthogonality condition is fulfilled automatically. The constraint (87) is respected by means of introducing real chemical potential $\lambda \to \infty$ for Abrikosov's auxiliary fermions or imaginary chemical potentials $\mu_t = -i\pi T/3$ for Popov-Fedotov semi-fermions (see details in [91]). The advantage of semi-fermionic representation is that it allows to construct a real-time Schwinger-Keldysh formalism [91] necessary for description of strongly non-equilibrium effects in systems with dynamical symmetries.

The fermionic representation of $SO(5)$ group is easily constructed by use of Hubbard operator representation and is characterized by 5-vector $\mathbf{q}^T = (f^\dagger_{-1} f^\dagger_0, f^\dagger_1, f^\dagger_s, f^\dagger_r)$

$$\begin{aligned} S^+ &= \sqrt{2}(f^\dagger_0 f_{-1} + f^\dagger_1 f_0), \quad S^z = f^\dagger_1 f_1 - f^\dagger_{-1} f_{-1}, \\ R^+ &= \sqrt{2}(f^\dagger_1 f_s - f^\dagger_s f_{-1}), \quad R^z = -(f^\dagger_0 f_s + f^\dagger_s f_0), \\ P^+ &= \sqrt{2}(f^\dagger_1 f_r - f^\dagger_r f_{-1}), \quad P^z = -(f^\dagger_0 f_r + f^\dagger_r f_0). \end{aligned} \tag{88}$$

and

$$A = i(f^\dagger_r f_s - f^\dagger_s f_r)$$

The constraint

$$n_1 + n_0 + n_{-1} + n_s + n_r = 1 \tag{89}$$

is respected either by real infinite chemical potential (Abrikosov pseudofermions) or by set of complex chemical potentials (semi-fermions). We do not present here ten 5×5 matrices characterizing $SO(5)$ representation to save a space. The reader can easily construct them using representations (10) or (88). There exists also a bosonic representation based on Schwinger bosons which might be derived by the method similar to used above for $SO(4)$ group.

The representations of higher $SO(n)$ groups can be constructed in a similar fashion. We address the reader to the papers [33] for further details of systematic classifications of $SO(n)$ groups where numerous examples of application of higher dynamical groups for quantum dots can also be found.

Kinematic constraints imposed on auxiliary fermions and bosons is in strict compliance with the Casimir and orthogonality constraints in spin space. Accordingly, the number of fermionic and bosonic fields reproduces the dimensionality of spin space reduced by these constraints. We have seen that the 6-D space of generators of $SO(4)$ group is reduced to D=4. Then the minimal (unconstraint) fermionic representation for this group should contain two $U(1)$ fermions. This means that the representation (87) is not minimal. Apparently, the best way to find such representation is to use Jordan-Wigner-like transformation [93]. The same kind of arguments applied to $SO(5)$ group tells us that the spinor field should contain seven components. This means that the representation (88) should be completed by one more (Majorana) fermion, and this fact points to one more hidden Z_2 symmetry [93].

7 Conclusion

The concept of dynamical symmetry in quantum mechanics has been (probably) first noted in the hydrogen atom and the isotropic harmonic oscillator. In these systems, there is a high degree of degeneracy of energy levels, which cannot be explained merely on the basis of rotational symmetry of the relevant Hamiltonian. In 50-es and 60-es the approach based on the ideas of dynamical symmetry was a powerful tool in high energy physics in an extremal situation, when the theoreticians had no relevant Lagrangian for description of experimentally observed hadron multiplets, but the symmetry of the system could be restored by group-theoretical methods, namely by constructing corresponding dynamical algebras.

Today, the concept of dynamical symmetry is ubiquitous in many branches of modern physics, such as quantum field theory, nuclear physics, quantum optics and condensed matter physics in low dimensions. Quantum dots are especially suitable objects for the group theoretical approach because the fully discrete spectrum of low-lying excitations in these systems often may be characterized by the definite dynamical symmetry, and the interaction with the metallic reservoir of metallic electrons in the leads provides a powerful tool of symmetry breaking.

In this review we concentrated on the spin excitations in quantum dots. Another promising class of nanoobject for applications of these ideas is spin ladders. In this case the role of object with definite dynamical symmetry is played by a single rung or pair of neighboring rungs bound by diagonal bonds, whereas the longitudinal modes violate this symmetry. The application of of dynamical symmetry approaches in this field are seldom enough as yet [94, 95], but the field seems to be really wide.

One more field for application of ideas developed in this review is the rapidly developing area of molecular electronics [96]. In artificially fabricated 2D molecular electronic circuits individual organic molecules are incorporated in electronic devices as basic elements. Molecular bridges containing one or several molecular groups and bound by tunnel contact with the rest network are the potential objects for description in terms of dynamical symmetry. Especially interesting is the case when the magnetic ions are caged within such a molecular group. One may expect manifestations of Kondo effect in current-voltage characteristics of such objects and indeed, first observations of Kondo resonances in tunnelling through metallorganic molecules are available [97]. In such objects the continuous symmetry of spin groups should be combined with discrete symmetry of finite rotation groups, which characterize the molecular symmetry. Possible involvement of vibrational degrees of freedom open new horizons for studies of dynamical symmetry at finite frequencies.

At the end, we hope to convince the reader of the beauty and relevance of dynamical symmetries in condensed matter physics and to stress its relation with down to earth experiments which, following the impressive technological fabrication techniques, can be performed in numerous laboratories.

ACKNOWLEDGMENTS

We are grateful to L.W.Molenkamp and M.Heiblum for discussion of various experimental aspects of nanophysics. This work is supported by the DFG under SFB-410 project, ISF grant, A.Einstein Minerva Center and the Transnational Access Program # RITA-CT-2003-506095. MK acknowledges support through the Heisenberg program of the DFG and U.S. DOE, Office of Science, under Contract No. W-31-109-ENG-39.

References

[1] E.P. Wigner, *Group Theory and its Applications to Quantum Mechanics*, (Academic Press, N.Y., 1959); M. Hammermesh, *Group Theory* (Addison-Wesley, 1962); R.S. Knox and A. Gold, *Symmetry in Solid State* (Benjamin, N.Y., 1964).

[2] I.A. Malkin and V.I. Man'ko, *Dynamical Symmetries and Coherent States of Quantum Systems* (Fizmatgiz, Moscow 1979) (in Russian).

[3] M.J. Englefield, *Group Theory and the Coulomb Problem* (Wiley, New York, 1972).

[4] V.A. Fock, Zs. Phys. **98**, 145 (1935); W. Bargmann, Zs. Phys. **99**, 576 (1936).

[5] J. Hubbard, Proc. Roy. Soc. A **285**, 542 (1965); see also Yu.P. Irkhin, Sov. Phys. - JETP **50**, 379 (1966).

[6] F.P. Onufrieva, Sov. Phys. JETP **53**, 1241 (1981); **59**, 986 (1984).

[7] Q.-y. Ye, R. Tsui and E.H. Nicollian, Phys. Rev. B**44**, 1806 (1991).

[8] M.G. Bawendi, W.L. Wilson, L. Rothberg, P.J. Carrol, T.M. Jedju, M.L. Steigerwald, and L.E. Brus, Phys. Rev. Lett., **65**, 1623 (1990); V. Petrova-Koch, T. Muschik, A. Kux, B.K. Meyer, F. Koch, and V. Lehmann, Appl. Phys. Lett. **61**, 943 (1992).

[9] D. Leonhard, M. Krishnamurthi, C.M. Reaves, S.P. Denbaars, and P.M. Petroff, Appl. Phys. Lett. **63**, 3203 (1993).

[10] L.P. Kouwenhoven, T.H. Oosterkamp, M.W.S. Danoesastro, M. Eto, D.G. Austing, T. Honda, and S. Tarucha, Science, **278**, 1788 (1997).

[11] M.A. Read and W.P. Kirk, *Nanostructure Physics and Fabrication* (Academic Press, Boston, 1989); M.A. Kastner, Phys. Today, **46**, 26 (1993).

[12] A. Lorke and R.J. Luyken, Physica B **256**, 424 (1998).

[13] L.W. Molenkamp, K. Flensberg, and M. Kemerlink, Phys. Rev. Lett. **75**, 4282 (1995); F. Hofmann, T. Heinzel, D.A. Waram, J.P. Kotthaus, G. Böm, W. Klein, G. Tränkle, and G. Weimann, Phys. Rev. B **51**, 13872 (1995); T.H. Oosterkamp, T. Fujisawa, W.G. van der Wiel, K. Ishibashi, R.V. Hijman, S. Tarucha, and L.P. Kouwenhoven, Nature **395**, 873 (1998).

[14] I.O. Kulik and R.I. Shekhter, Sov. Phys.–JETP, **41**, 308 (1975); L.I. Glazman and R.I. Shekhter, J. Phys.: Condens. Matter **1**, 5811 (1989)

[15] *Single Charge Tunnelling*, eds. H. Grabert and M.H. Devoret (Plenum, New York, 1992).

[16] S. Tarucha, D.G. Austing, T. Honda,, R.G. van der Hage and L.P. Kouwenhoven, Phys. Rev. Lett. **77**, 3613 (1996).

[17] V.A. Fock, Z. Phys. **47**, 446 (1928); C.G. Darwin, Proc. Cambridge Philos. Soc. **27**, 86 (1930).

[18] M. Wagner, U. Merkt, and A.V. Chaplik, Phys. Rev. B **45**, 1951 (1992); B. Jouault, G. Santoro, A. Tagliacozzo, Phys. Rev. B **61**, 10243 (2000).

[19] D. Giuliano, B. Jouault and A. Tagliacozzo, Europhys. Lett. **58**, 401 (2002).

[20] A. Wojs, et al, Phys. Rev. B **54**, 5604 (1996); H. Jiang and J. Singh, Phys. Rev. B **56**, 4696 (1997); J. Kim, L-W. Wang, and A. Zunger, Phys. Rev. B **57**, 9408 (1998) and referencers therein.

[21] U. Banin, Y-W. Gao, D. Katz, and O. Millo, Nature **400**, 542 (1999).

[22] K. Brunner, G. Abstreiter, G. Böhm, G. Tränkle, and G. Weimann, Phys. Rev. Lett. **73**, 1138 (1974); M. Bayer, et al, Phys. Rev. B **58**, 4740 (1998).

[23] S. Raimond, P. Hawrylak, C. Gould, S. Fafard, A. Sachrajda, M. Potemski, A. Wojs, S. Charbonneau, D. Leonard, P.M. Petroff, and J.L. Merz, Solid State Commun. **101**, 883 (1997)

[24] M. Bayer, O. Stern, P. Hawrylak, S. Fafard, and A. Forchel. Nature **405**, 923 (2000); P. Hawrylak, Solid State Commun. **127**, 793 (2003).

[25] I.V. Lerner and Yu.E. Lozovik, Sov. Phys. JETP **53**, 763 (1981); A.B. Dzyubenko and Yu. E. Lozovik, Sov. Phys.-Solid State **25**, 874 (1983); *ibid* **26**, 938 (1983); A.B. Dzyubenko and Yu.E. Lozovik, J. Phys. A **24**, 415 (1991).

[26] K. Kikoin and Y. Avishai, Phys. Rev. Lett. **86**, 2090 (2001); Phys. Rev. **B65**, 115329 (2002).

[27] L. Borda, G. Zarand, W. Hofstetter, B.I. Halperin, and J. von Delft, Phys. Rev. Lett. **90**, 026602 (2003).

[28] T. Pohjola, H. Schöller, and G. Schön, Europhys. Lett. **55**, 241 (2001).

[29] E. Lebanon, A. Schiller, and F. Anders, Phys. Rev. B **68**, 155301 (2003).

[30] J.J. Palacios and P. Hawrylak, Phys. Rev. B **51**, 1769 (1995).

[31] B. Partoens and F.M. Peeters, Phys. Rev. Lett. **84**, 4433 (2000).

[32] E. Anisimovas and F.M. Peeters, Phys. Rev. B **65**, 233302 (2002); **66**, 075311 (2002).

[33] T. Kuzmenko, K. Kikoin and Y. Avishai, Phys. Rev. Lett. **89**, 156602 (2002); Phys. Rev. B **69** 195109 (2004).

[34] J. Appelbaum, Phys. Rev. Lett. **17**, 91 (1966).

[35] L.I. Glazman and M.E. Raikh, JETP Lett. **47**, 452 (1988); T.K. Ng and P.A. Lee, Phys. Rev. Lett. **61**, 1768 (1988).

[36] D. Goldhaber-Gordon, H. Shtrikman, D. Mahalu, D. Abush-Magder, U. Meirav, and M.A. Kastner, Nature **391**, 156 (1998); S.M. Cronenwett, T.H. Oosterkamp, and L.P. Kouwenhoven, Science **281**, 540 (1998); F. Simmel, R.H. Blick, J.P. Kotthaus, W. Wegscheider, and M. Bichler, Phys. Rev. Lett. **83**, 804 (1999).

[37] W.G. van der Wiel, S. de Francheschi, T. Fujisawa, J.M. Elzerman, S.Tarucha, and L.P. Kowenhoven, Science **289**, 2105 (2000).

[38] J. Nygård, D.H. Cobden and P.E. Lindelof, Nature **408**, 342 (2000).

[39] N S. Sasaki, S. De Franceschi, J.M. Elzermann, *et al.,* Nature, **405**, 764 (2000).

[40] M. Pustilnik, Y. Avishai and K. Kikoin, Phys. Rev. Lett. **84**, 1756 (2000).

[41] D. Giuliano and A. Tagliacozzo, Phys. Rev. Lett. **84**, 4677 (2000); D. Guiliano, B. Jouault, and A. Tagliacozzo, Phys. Rev. **63**, 125318 (2000)

[42] M. Eto and Yu. Nazarov, Phys. Rev. Lett. **85**, 1306 (2000), Phys. Rev. B **64**, 085322 (2001).

[43] A.C. Hewson, *The Kondo Problem to Heavy Fermions* (Cambridge University Press, 1997).

[44] J.R. Schrieffer and P.A. Wolff, Phys. Rev. **149**, 491 (1966).

[45] A.M. Tsvelick and P.B. Wiegmann, Adv. Phys. **32**, 453 (1983).

[46] A.A. Abrikosov, Physics, **2**, 5 (1965)

[47] A.A. Abrikosov and A.A. Migdal, J. Low Temp. Phys. **3**, 519 (1970).

[48] M. Fowler and A. Zawadovski, Solid State Commun. **9**, 471 (1971).

[49] D.Cox and A. Zawadovski, Adv. Phys. **47**, 599 (1998).

[50] P.W. Anderson, J. Phys. C **3**, 2436 (1970).

[51] F.D.M. Haldane, Phys. Rev. Lett. **40**, 416 (1978).

[52] A. Kaminski, Yu. V. Nazarov, and L.I. Glazman, Phys. Rev. B **62**, 8154 (2000).

[53] I. Affleck and A.W.W. Ludwig, Phys. Rev. B **48**, 7297 (1993).

[54] M. Pustilnik and L. Glazman, Phys. Rev. Lett. **85**, 2993 (2000), Phys. Rev. B **64**, 045328 (2001).

[55] J. Kyriakidis, M. Pioro-Ladriere, M. Ciorga, A.S. Sachrajda, and P. Hawrylak, Phys. Rev. B **66**, 035320 (2002).

[56] A. Kogan, G. Granger, M.A. Kastner, and D. Goldhaber-Gordon, Phys. Rev. B **67**, 113309 (2003).

[57] A. Fuhrer, T. Ihn, K. Ensslin, W. Wegscheider, and M. Bichler, Phys. Rev. Lett. **91**, 206802 (2003).

[58] W. Hofstetter and H. Schoeller, Phys. Rev. Lett. **88**, 016803 (2002).

[59] M. Vojta, R. Bulla, and W. Hofstetter, Phys. Rev. B **65**, 140405 (2002).

[60] M. Pustilnik and L. Glazman, Phys. Rev. B **64**, 045328 (2001).

[61] M. Pustilnik and L. Glazman, Phys. Rev. Lett. **87**, 216601 (2001).

[62] M. Pustilnik, L. Glazman, and W. Hofstetter, Phys. Rev. B **68**, 161303 (2003); W. Hofstetter and G. Zarand, Phys. Rev. B **69**, 235301 (2004).

[63] P. Nozieres and A. Blandin, J. Phys. (Paris) **41**, 193 (1980).

[64] K.G. Wilson, Rev. Mod. Phys. **47**, 773 (1975); T.A. Costi, A.C. Hewson, and V. Zlatić, J. Phys.: Cond Mat. **6**, 2519 (1994); W. Hofstetter, Phys. Rev. Lett. **85**, 1508 (2000).

[65] B.A. Jones and C.M. Varma, Phys. Rev. Lett. **61**, 125 (1988); B.A. Jones, C.M. Varma, and J.W. Wilkins, *ibid.* **61**, 125 (1988); B.A. Jones and C.M. Varma, Phys. Rev. B **40**, 324 (1989).

[66] V.I. Melnikov, JETP Lett. **35**, 511 (1982).

[67] D.C. Langreth, Phys. Rev. **150**, 516 (1966).

[68] S.D. Glazek and K.G. Wilson, Phys. Rev. D **48**, 5863 (1993); F. Wegner, Ann. Physik (Leipzig), **3**, 77 (1994).

[69] M.H. Hettler and H. Schoeller, Phys. Rev. Lett. **74**, 4907 (1995); T-K. Ng, Phys. Rev. Lett. **76**, 487 (1996); A. Schiller and S. Hershfield, Phys. Rev. Lett. **77**, 1821 (1996); Y. Goldin and Y. Avishai, Phys. Rev. Lett. **81**, 5394 (1998); Y. Goldin and Y. Avishai, Phys. Rev. B **61**, 16750 (2000).

[70] G. Platero and R. Aguado, Phys. Reports **395**, 1 (2004).

[71] K. Kikoin and Y. Avishai, Phys. Rev. B **62** 4647 (2000).

[72] T. Fujii and N. Kawakami, Physica B **281&282**, 406 (2000); Phys. Rev. B **63**, 064414 (2001).

[73] G. Mahan, Phys. Rev. **163**, 612 (1967); P. Nozieres and C. DeDominicis, Phys. Rev. **178**, (1969); S. Doniach and M. Sunjic, J. Phys. C **3**, 285 (1970).

[74] T.V. Shahbazyan, I.E. Perakis, and M.E. Raikh, Phys. Rev. Lett. **84**, 5896 (2000).

[75] A.O. Govorov, K. Karrai, and R.J. Warburton, Phys. Rev. B **67**, 241307 (2003).

[76] R.J. Warburton, C. Schäflein, D. Haft, F. Bickel, A. Lorke, K. Karrai, J.M. Garcia, W. Schoenfeld, and P.M. Petroff, Nature, **405**, 926 (2000).

[77] K. Karrai, R.J. Warburton, c. Schullhauser, A. Högele, B. Urbaszek, E.J. McGhee, A.O. Govorov, J.M. Garcia, B.D. Gerardot, and P.M. Petroff, Nature, **427**, 135 (2004).

[78] S. Hershfield, J.H. Davies, and J.W. Wilkins, Phys. Rev. Lett. **67**, 3720 (1991); Y. Meir, N.S. Wingreen and P.A. Lee, Phys. Rev. Lett. **70**, 2601 (1993); T.K. Ng, Phys. Rev. Lett. **70**, 3635 (1993), N.S. Wingreen and Y. Meir, Phys. Rev. B **49**, 11040 (1994).

[79] A. Rosch, J. Kroha, and P. Wölfle, Phys. Rev. Lett. **87**, 156802 (2001); A. Rosch, J. Paaske, J. Kroha, and P. Wölfle, Phys. Rev. Lett. **90**, 076804 (2003); J. Paaske, A. Rosch, J. Kroha, and P. Wölfle, Phys. Rev. B **69**, 155330 (2004).

[80] M.N. Kiselev, K. Kikoin and L.W. Molenkamp, JETP Letters **77**, 434 (2003); Phys. Rev. B **68** 155323 (2003).

[81] O. Parcollet, C. Hooley, Phys. Rev. B **66**, 085315 (2002); W. Mao, P. Coleman, C. Hooley, and D. Langreth, Phys. Rev. Lett. **91**, 207203 (2003).

[82] J. Paaske, A. Rosch, P. Woelfle, N. Mason, C.M. Marcus, and J. Nygard, arXiv:cond-mat/0603581, Nature Physics (2006), in press.

[83] B.Wybourne, *Classical Groups for Physicists*, Willey, New York, 1974.

[84] L.D. Landau and E.M. Lifshitz, *Quantum Mechanics (Non-relativistic Theory)*, Pergamon Press, London, 1959.

[85] The hidden symmetry becomes explicit for a symmetric rotator characterized by the Hamiltonian $\mathcal{H} = (2I_3)^{-1}\mathbf{L}^2 + [(2I_1)^{-1} - (2I_3)^{-1}]\mathbf{M}^2$.

[86] M. Abramovitz and I. Stegun, *Handbook of Mathematical Functions*, Dover Publications, New York, 1965.

[87] A. Perelomov, *Generalized Coherent States and Their Applications*, Springer, Berlin, 1986.

[88] J. Schwinger, in *Quantum Theory of Angular Momentum*, L.C. Biedenharn and H. van Dam, Eds., Academic Press, New York, 1965, pp. 229-279.

[89] V.N. Popov and S.A. Fedotov, Sov. Phys. JETP **67**, 535 (1988).

[90] M.N. Kiselev, H. Feldmann and R. Oppermann, Eur. Phys. J. **B 22**, 53 (2001).

[91] M.N. Kiselev, R. Oppermann, Phys. Rew. Lett. **85**, 5631 (2000).

[92] Chou-Cheng Zhang, Science **275**, 1089 (1997).

[93] A.M. Tsvelik, *Quantum Field Theory in Condensed Matter Physics*, Cambridge Unversity Press, Cambridge, 1995.

[94] K. Kikoin, Y. Avishai and M.N. Kiselev. *Explicit and hidden symmetries in quantum dots and quantum ladders*, in *"Molecular Nanowires and other Quantum Objects"* (eds. A.S. Alexandrov and R.S. Williams), NATO Sci. Series, vol. 148 pp. 177-189 (2004).

[95] C.D. Batista and G. Ortiz, Phys. Rev. Lett. 85, 4755 (2001), Advances in Physics, **53**, 1 (2004).

[96] C. Joachim, J.K. Gimzewski, and A. Aviram, Nature **408**, 541 (2000); A. Nitzan and M.A. Ratner, Science **300**, 1384 (2003); Y.Q. Xue and M.A. Ratner, Phys. Rev. B **69**, 085403 (2004), and references therein.

[97] J. Park, A.N. Pasupathy, J.I. Goldsmith, C. Chang, Y. Yaish, J.R. Petta, M. Rinkoski, J.P. Sethna, H.D. Abruna, P.L. Mceuen, and D.C. Ralph, Nature **417**, 722 (2002); W. Liang, M.P. Shores, M. Bockrath, J.R. Long, and H. Park, Nature **417**, 725 (2002).